Relindis Rott

Reconnection Events in the Near-Earth Magnetotail using Cluster Data

MASTER THESIS

For obtaining the the academic degree
Diplom-Ingenieurin

Diploma Program of Technical Physics

Graz University of Technology

Supervisor:
Ao.Univ.-Prof. Dipl.-Ing. Dr.phil Martin Heyn
Institute of Theoretical and Computational Physics

in cooperation with
Space Research Institute
Austrian Academy of Sciences

Graz, October 2010

Abstract

Reconnection-Events in the Near-Earth Magnetotail using Cluster Data

In this study data of ESA's Cluster Mission are evaluated to find reconnection events in the near-Earth magnetotail. Cluster is a multi-spacecraft mission which uses 4 satellites forming a tetrahedron designed to observe small scale processes in the magnetosphere. During the tail season of the mission from July to October, the tetrahedral formation of Cluster crosses the central magnetotail. Data are evaluated for the period 2001 to 2007. For an automatic search procedure within this huge data set, appropriate search criteria have been formulated and tested. The main signatures of reconnection are characteristic changes of the magnetic field structure and the appearance of accelerated plasma flows. The whole procedure yields 50 events which passed the criteria for reconnection. From a statistical analysis of the selected events it is concluded that the majority of events shows a tailward propagating x-line. This is indicated by the sequence of high-speed flow directions. In addition, earthward flows seem to occur with higher velocities than tailward flows. The thickness of the tail current sheet, evaluated from the results, is shown to be in agreement with the selected criteria in the automatic search routine.

Kurzfassung

Reconnection-Ereignisse im erdnahen Magnetschweif mittels Cluster Daten

In dieser Arbeit werden Daten von ESA's Cluster Mission ausgewertet um Reconnection-Ereignisse im erdnahen Magnetschweif zu finden. Cluster ist eine Multi-Satelliten Mission, welche mittels 4 Satelliten einen Tetraeder formt, entwickelt um Prozesse geringer Größenordnung in der Magnetosphäre zu beobachten. Von Juli bis Oktober kreuzt die Cluster-Formation den zentralen Magnetschweif. Daten werden für den Zeitraum von 2001 bis 2007 ausgewertet. Um in diesem großen Datensatz eine automatisierte Suche durchzuführen, werden passende Kriterien formuliert und getestet. Die besondere Signatur der Reconnection besteht aus charakteristischen Änderungen des Magnetfeldes zusammen mit dem Auftreten beschleunigter Plasmaströmungen. Der gesamte Suchvorgang liefert 50 Ereignisse, welche die typischen Charakteristika von Reconnection aufweisen. Die statistische Analyse dieser 50 Ereignisse zeigt, dass die Mehrheit der Ereignisse eine sich schweifwärts bewegende X-Linie aufweist. Dies ist erkennbar an der Abfolge der Strömungsrichtungen des Plasmas hoher Geschwindigkeit. Zusätzlich zeigen die erdwärts gerichteten Plasmaströme höhere Geschwindigkeiten als die schweifwärts gerichteten Ströme. Die Dicke der Stromschicht, die mittels der Ergebnisse ausgewertet wurde, stimmt überein mit den ausgewählten Kriterien der automatisierten Suche.

Contents

Chapter 1

Introduction

Plasma is a state of matter, which contains charged particles. Negative and positive charges are present in equal numbers, to restore quasineutrality of the entire gas. The plasma state can be interpreted as the 4^{th} state of matter after solid, liquid, and gaseous, even though it is not a phase transition of 1st order. A gas at extremely high temperatures turns into a plasma, because atoms and molecules are ionized with increasing temperature. The temperature has to be sufficiently high to overcome strong Coulomb forces, which try to counteract the decoupling. These forces lead to a collective behavior of free particles.
On the Earth's surface the plasma state is rare, and can be found in lightnings or flames. In the universe and near-Earth space 99% of all matter is in the plasma state. There are various different types of plasmas depending on temperature, density, and other characteristic parameters. Plasma can carry electric currents and is sensitive to electric and magnetic fields. In space its behavior is less determined by gravity or collisions, but instead governed by these fields.

The research on plasma physics has currently several fields. One is the understanding of natural plasmas in space, like plasma inside of stars or in near-Earth space. Another is to generate plasma in laboratory and to possibly activate fusion as a possible future source of energy.
While the measurement-methods of laboratory-plasmas are numerous, space plasmas are more difficult to detect. In near-Earth space at least measurements from satellites are available. It is actually a perfect natural lab for plasma physics. The beginning of this research was initiated long ago by 2 main components: the geomagnetic field and the beautiful aurora phenomenon.

With the invention of the compass the Earth's magnetic field was discovered. Much earlier the aurora phenomenon had already been observed and appeared in literature in ancient times. The connection between these 2 was first suggested by Edmund Halley. He believed that the aurora was directed along the geomagnetic field.
1878 Henri Becquerel proposed a similar theory. Particles ejected from sunspots were guided by the geomagnetic field, finally causing aurora.
Some years later in 1897 Kristian Birkland started his groundbreaking work on geophysics with the first of three expeditions to northern Norway, to view aurora. From the data he deduced that during aurora large electric currents were

flowing along geomagnetic field lines.
Together with the invention of the vacuum tube and the discovery of electrons, he was able to create a lab experiment of a magnetic dipole field inside a sphere, an Earth-model. Electrons on the so called terella produced patterns, resembling to the auroral zone. A Norwegian mathematician performed some calculations on that dipole field and found the first hints of the radiation belts.
At the beginning of the 20^{th} century the ionosphere was postulated, to explain transatlantic radio transmissions and later verified with its 3 layers, D, E and F.
The disturbances of geomagnetic field strength, detected on the ground, were in 1918 considered by Sydney Chapman as effect of a single charged beam coming from the sun. This idea was corrected by F. Lindemann. A single charged beam would be destroyed by electrostatic repulsion. The beam must be composed of charges of both signs in equal numbers. The occurrence of a plasma was suggested for the first time.
Then Chapman and Ferraro established the picture of solar plasma compressing the geomagnetic field when it approaches the Earth, forming a cavity, which is surrounded by the plasma. The magnetosphere was found.
The increase and subsequent decrease of the magnetic field strength was explained for the first time, today called a geomagnetic storm. In the 1950s the exploration of the magnetosphere with the help of rockets and later satellites began and led to rapidly increasing knowledge in that field. The bow shock, as a shock of collisionless plasma in space was an interesting discovery and difficult to explain at first. Electric and magnetic fields can act to a plasma in a way similar to the effect of collisions.
Reconnection in the magnetosphere was proposed by James Dungey in 1961, as an effect at the magnetopause on the dayside, linking field lines of the geomagnetic field to the interplanetary magnetic field. The flux of solar wind plasma is transported to the nightside until the second site of reconnection in the tail is activated. All this is discussed more in detail in chapter 3.

Two co-orbiting satellites, ISSE 1 and 2, found the first evidence of reconnection, when detecting accelerated plasma flows at the locations of interest, the magnetopause and the magnetotail.
The reconnection phenomenon is a very complex process. To detect it and make reasonable interpretation possible, more than 2 satellites are needed. The Cluster mission provides the means of a whole Cluster, consisting of 4 satellites flying in formation, detecting reconnection and other processes in key regions. Still there are many, partly inconsistent theories about reconnection and a lot of research is done on this topic.
In this thesis the search of reconnection events in Cluster data and their interpretation is the main aim. A description of the Cluster mission can be found in the following chapter 2.
Encountered events dedicated to reconnection are discussed in the data-analysis.

In a reconnection process magnetic field energy is converted into plasma acceleration. Maybe in the future knowledge about reconnection could be used in other fields of plasma physics or other applications.

Chapter 2

The Cluster Mission

2.1 Cluster Mission

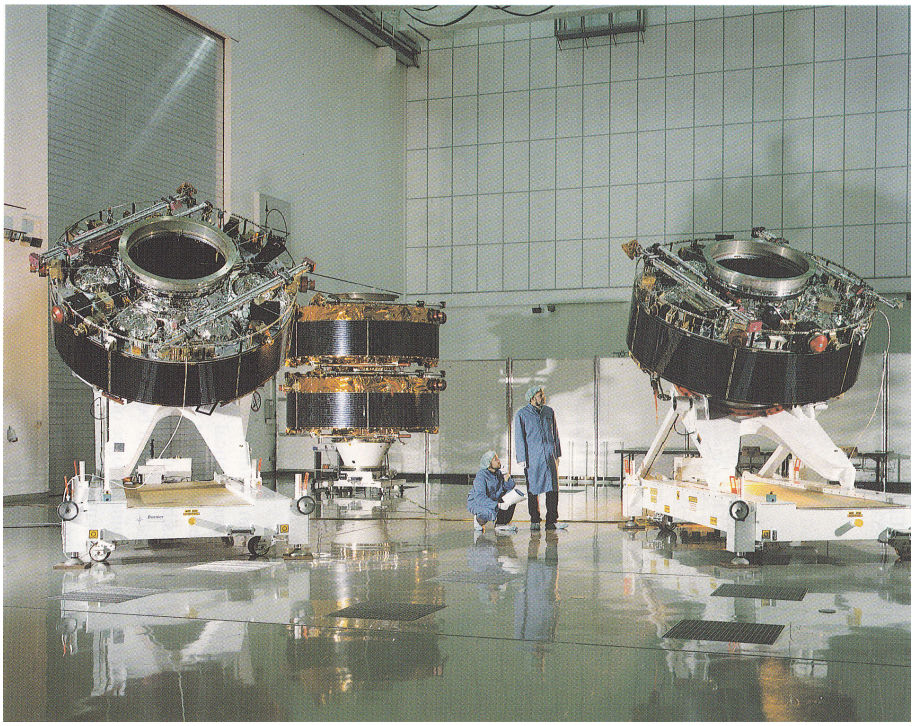

Figure 2.1: All 4 spacecraft of the Cluster mission [Esa]. [ERS97]

The Cluster Mission is a multi-spacecraft mission, composed of 4 spacecraft, each identically equipped with eleven instruments for measuring scientific data. The mission was first proposed in 1982 and after its pre-development presented to the scientific community in 1985. In 1986 the ESA Science Program Committee selected the mission together with the SOHO Mission in their Solar Terrestrial Science Program (STSP).

The tetrahedral configuration was the idea of a French study and provides the ability to measure small-scale plasma characteristics and its temporal and spacial variations (in 3 dimensions). It was meant to view magnetospheric characteristics, in both the polar cusp and magnetotail region, and the near-Earth solar wind plasma. Therefore a suitable orbit plane was chosen to fulfill these requirements.

The Cluster was launched in 1996 by the new built Ariane-5 rocket at Korou, French Gujana, during its maiden flight. Unfortunately the rocket was self-destructed, when it came off course, due its intense aerodynamic loads, in less then a minute after take off. All 4 Cluster spacecraft on board were destroyed.
After many considerations about how to rebuild the mission to meet its scientific goals, it was decided to build 3 of the spacecraft completely new and the 4th out of spare parts of the old mission. The latter was called Phoenix after the famous bird arising from its ashes.

As a result of a public competition the spacecraft were renamed as Salsa, Samba, Tango and Rumba.
On 16^{th} of July 2000 the first 2 spacecraft of the Cluster Mission were launched. On 9^{th} of July the remaining 2 were launched. Both flights operated by a Soyuz at Baikonur, Kasakhstan.

Each spacecraft is of cylindrical shape, 1.3 m high and 2.9 m in diameter. It carries 6 spherical fuel tanks and 8 thrusters for small changes of orbit. The electrical power supply consists of 6 curved solar panels around the cylinder and 5 batteries used during shadow transits.
Rod-shaped booms provide 2 antennas for communication, 2 sensors and 4 wire booms operate as the spacecraft spins to measure the changing magnetical and electrical fields.

The main goal is to measure small-scale plasma structures, their size and shape, varying in time and 3-dimensional space in the key regions. These are the bow shock, the magentopause, the polar cusp, the magnetotail and the auroral zone.
The spacecraft were launched into coordinated polar orbits forming a tetrahedron with an apogee of 19.6 Earth-radii (R_E) and a perigee of $4\,R_E$ in 2000 and an orbital period of 57 hours. By crossing the plasma structures in a tetrahedral formation a time resolution as well as a 3 dimensional resolution becomes possible and it can be distinguished between temporal and spatial variation.

The first 4 years the orbits were maintained, with an apogee near the ecliptic plane that causes the spacecraft to pass the plasma sheet at about $19\,R_E$ during a tail crossing. In this region, at the apogee in the Earth's magnetotail, they were forming a regular tetrahedron, whichs scale varied every 6 months, hence each tail season (August to October).
In 2005 the strategy was changed. The regular tetrahedron-formation was abandoned. Instead Cluster 1, 2 and 3 were navigated into a triangular plane, separated 10 000 km from each other, while the distance of spacecraft 3 and 4 was 1000 km perpendicular to the plane. The line of apsides proceeded toward the

south pole making the Custer tetrahedron crossing the plasma sheet closer and closer to the Earth each season.
In 2006 the spacecraft were again forming a regular tetrahedron, separated 10 000 km from each other.
From 2007 on the multi scale strategy was readopted. It was proposed to find a link between phenomena at different spatial scales.

Year	Tetrahedron Scale Size [km]
2001	2000
2002	4000
2003	200
2004	1000
2005	multi scale: 10 000, 1000
2006	10 000
2007	multi scale: 10 000, 40
2008	multi scale: 10 000, 3000
2009	multi scale: 10 000, 500

Table 2.1: Inter spacecraft separation during central magnetotail crossing

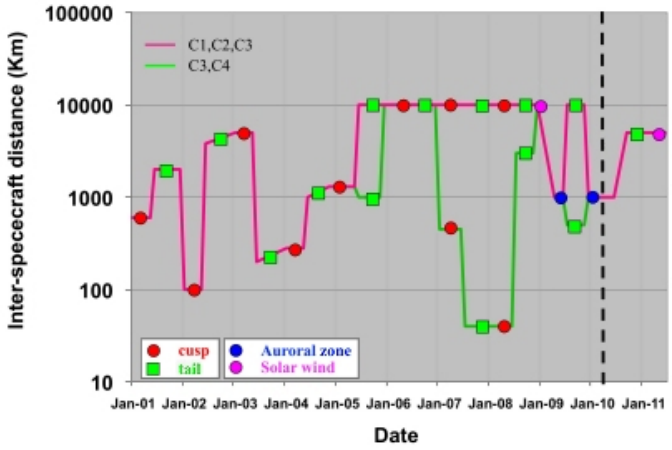

Figure 2.2: Inter Spacecraft separation 2010. From [esa]

The scientific measurements started in February 2001. The mission was originally planned to end in 2003 but has been extended several times, eventually until 2012.

2.1.1 Instrumentation on Board

Here are the main components and short descriptions of the experiments on board of each Cluster-spacecraft.

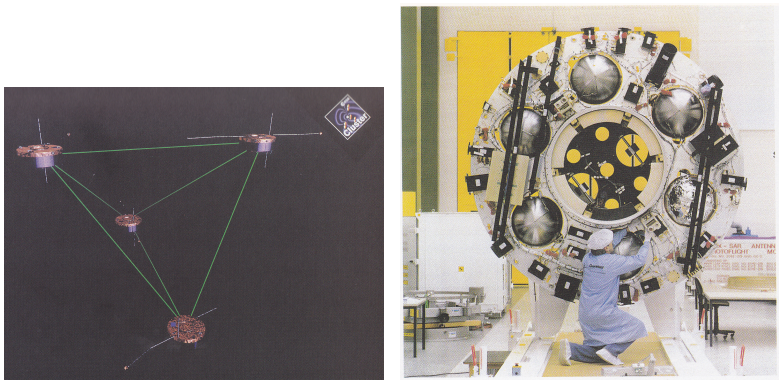

Figure 2.3: Tetrahedral configuration and Cluster spacecraft [ERS97]

FGM *Fluxgate Magnetometer*
Measurement of magnetic field vector

CIS *Cluster Ion Spectrometry*
Measurement of full 3D ion distribution; 2 sensors consisting of:
CODIF *Composition and Distribution Function Analyser*
HIA *Hot Ion Analyser*
Precise measurement of both, the large flux ion beam of the solar wind and the low flux ions in lobes of the magnetosphere

EDI *Electron Drift Instrument*
Emission and subsequent detection of tracer electrons to derive ambient electrical field

PEACE *Plasma Electron and Current Experiment*
LEEA *Low Energy Electron Analyser*
HEEA *High Energy Electron Analyser*

EFW *Electrical Field and Wave*

STAFF *Spatio-Temporal Analysis of Field Fluctuations*

WHISPER *Waves of High frequency and Sounder for Probing of Electron density by Relaxation*

WBD *Wide Band Data*

DWP *Digital Wave Processing*

ASPOC *Active Spacecraft Potential Control*
To maintain electrostatic potential of spacecraft with respect to ambient plasma at low level

RAPID *Research with Adaptive Particle Imaging Detectors*
2 spectrometers; position-sensitive solid state detectors
IIMS *Imaging Ion Mass Spectrometer*
IES *Imaging Electron Spectrometer*

FGM and CIS are the basic instruments used in the following analysis. Combining the datasets, calculation of the electric field, with $\mathbf{E} = \mathbf{V} \times \mathbf{B}$, becomes possible as well. It can be used as additional parameter and compared to measured data from EDI.
WEC is short for Wave Experiment Consortium and includes all instruments used for wave detection: EFW, STAFF, WHISPER, WBD, DWP.
ASPOC includes an ion emitter. Emission of indium ions stabilizes the fluctuating potential.
RAPID additionally has a special mode for detection of neutral atoms.

2.1.2 Other Missions

There are also other missions closely linked to Cluster.

The Chinese **Double Star Program DSP** is one of these. It is a 2-spacecraft mission, with similar objectives and instruments like Cluster and was launched in 2003 and 2004 as a project of the Chinese National Space Administration (CNSA). It is operated in collaboration with ESA. One of its satellites, TC-1, is equatorial aligned (inclination 28° to the equator), the other, TC-2, is polar aligned (inclination 90° to the equator). Compared to Cluster, the Double Star orbits are closer to the Earth. Combining data from both, Cluster and Double Star, yields better insight in physical fundamentals.

The **Geotail Mission** was launched in 1992 as a collaboration of NASA and ISAS, the former Japanese space agency today known as JAXA. Its objective is to study the geotail over a wide range of distance in between 8-200 R_E. Until 1995 it spent most of its time in the distant tail, with an apogee on the nightside up to 200 R_E. In phase two the near-Earth observation was started and the apogee reduced to 30 R_E. It was designed to find out more about processes in the magnetosphere, especially the magnetopause, the plasma sheet and reconnection.

WIND was launched in 1994 as the first of 2 spacecraft. This NASA project focuses on plasma and energetic particles outside the magnetosphere, in the solar wind and was placed in an halo orbit around the Lagrange point L1, about 200 R_E sunward from Earth.

ACE is short for *Advanced Composition Explorer*, another NASA mission, launched in 1997 and placed also around L1, to study particle distributions over a wide range. It monitors high energy particles as well as low energy particles and provides information about the space weather. It also includes a warning system of geomagnetic storms.

THEMIS is a relatively young mission, started in 2007. The name stands for *Time History of Events and Macroscale Interactions during Substorms* and the mission consists of 5 identical spacecraft. In contrast to Cluster, they do not fly in formation, but are spread across the tail. The aim is to collect data during substorms, to find out more about the phenomenon of auroras and to gain insight into severe magnetic storms, to protect infrastructure and astronauts.

Chapter 3

Basic Principles

3.1 The Magnetosphere

Planet Earth has a core, part of it is from liquid iron. Its fluid flows and currents cause a magnetic field that stretches out far beyond the Earth's surface into space. This magnetic field is bound inside a barrier that separates it from an outer magnetic field which originates from the sun. The boundary separating both fields from each other is called magnetopause and the inner region containing the terrestrial magnetic field is the magnetosphere. The concept of the magnetosphere was first introduced by Chapman and Ferraro. They concluded that the solar wind flows around the Earth's magnetic field and confines it, forming a cavity, the magnetosphere.
The main components of the magnetosphere are

- magnetopause,
- plasma mantel,
- plasma sheet,
- neutral or current sheet,
- plasmasphere,
- ionosphere.

The influential structures outside the magnetosphere are

- bow shock,
- magnetosheath.

3.1.1 Magnetopause

The magnetopause separates the so called interplanetary magnetic field (IMF), originating from the sun, from the Earth's magnetic field, which from now on is referred to as planetary or terrestrial magnetic field .
It acts as an upper boundary of the magnetosphere and is not symmetrical

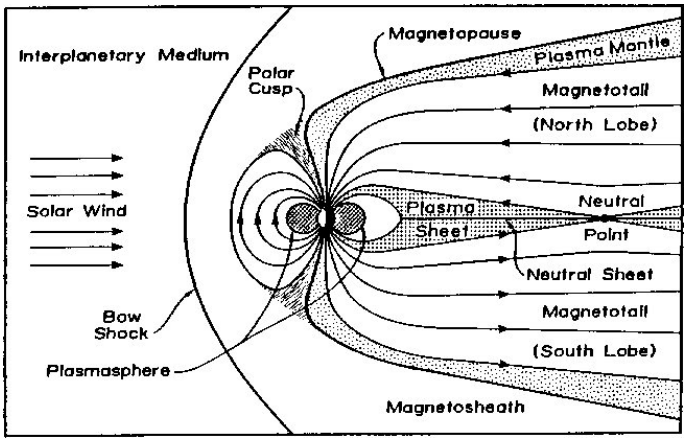

(a) Magnetosphere 2D in the noon-midnight meridional plane [RK95]

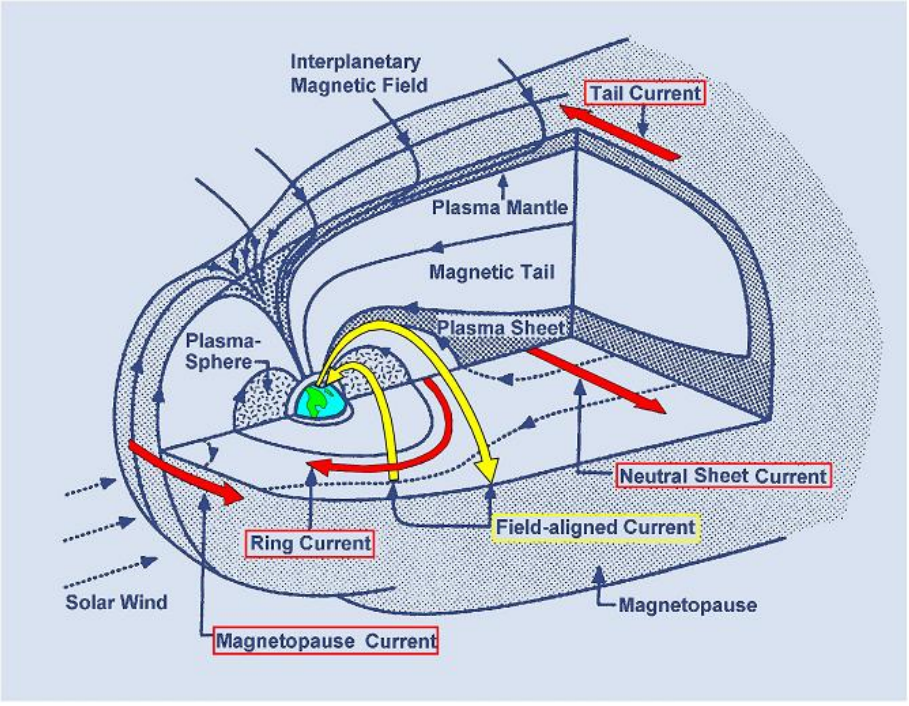

(b) Magnetosphere 3D. Picture from `http://www.geomag.us/info/magnetosphere.html`, modified from Kivelson and Russell (1995)

Figure 3.1: Magnetosphere

around the Earth, because the Earth and its magnetosphere is to the solar wind like an obstacle in space.
The solar wind is a flow of electrically charged particles, mainly H^+ and He^{++} ions, coming from the sun. It is a fully ionized plasma with a mean free path of about 1 astronomical unit (AU). In such a collisionless plasma coupling and transfer of momentum and energy is absent. It streams at a speed of about 400 km/s (ranging from 300 km/s to 800 km/s) and is pervaded by the IMF. When it approaches Earth it is deflected by the magnetosphere, which it cannot cross, gets decelerated, compressed and heated. This deceleration slows the solar wind down from supersonic to subsonic speed. This results in a shock wave standing in space in front of the magnetopause, the so called **bow shock**.

While a classical gas flow has a defined speed of sound, the exclusive velocity at which a sound wave can propagate, a plasma supports several types of waves and therefore several velocities. The terms super- and subsonic are in this context referring to one of those modes. The exact position of the magnetopause in space depends directly on the solar wind's plasma pressure and planetary magnetic field pressure inside the magnetopause. It is the surface where the plasma pressure of the solar wind and the magnetical field pressure from Earth are in equilibrium

$$P_{plasma} = P_{mag} \ , \tag{3.1}$$

$$P_{plasma} = \rho \ v^2 \qquad \text{plasma pressure,} \tag{3.2}$$

$$P_{mag} = \frac{B^2}{2\mu_0} \qquad \text{magnetic field pressure.} \tag{3.3}$$

Due to the fact that the solar wind is not a static quantity as well as the planetary magnetic field varies marginal with time, the surface changes position and moves toward and away from Earth from time to time. Depending on the solar activity it can be found at around 14 Earth radii (R_E) sunward from the Earth, in between the Earth and the sun and ranges up to several hundred R_E in the magnetotail, which is directed away from the sun, behind the Earth.

The solar wind flows around the magnetosphere at subsonic speed forming a region of turbulent plasma outside the magnetopause, the **magnetosheath**. The reason why the solar wind particles cannot enter the magnetosphere is the frozen-in flux concept, which will be discussed later on. Its violation gives rise to reconnection, a principle that allows magnetic field lines to be cut and reconnected to other partners of different origin and thus different plasma populations to mix.

3.1.2 Geomagnetic tail

The gemagnetic tail is the region directed away from the sun. It contains

- the plasma mantle,
- north and south lobe,
- plasma sheet,
- current sheet,

- x-line.

It is a reservoir of plasma and stretches out up to several hundred R_E.

The **north** and **south lobes** are regions of oppositely directed magnetic field lines. The northern lobe field is directed towards the Earth and connected to the magnetic north pole, while the south lobe field is directed away from the Earth as it is connected to the magnetic south pole. The interface that seperates these lobes carries electric currents, according to Ampère's law and thus is a **current sheet**, also called **neutral sheet** in this region

$$\nabla \times \mathbf{B} = \mu_0 \left(\mathbf{j} + \epsilon_0 \frac{\partial \mathbf{E}}{\partial t} \right) \ , \tag{3.4}$$

$$\Delta \mathbf{B} = \mu_0 \mathbf{I} \ . \tag{3.5}$$

The current sheet is relatively thin, compared to its other dimensions, and can be described as a plane. It is in the center of the tail, embedded in the much thicker **plasma sheet**, a region of hot plasma.
The plasma parameter β, which is the ratio of particle pressure P_p and magnetic field pressure P_B, differs depending on the region in the tail

$$\beta = \frac{P_p}{P_B} = \frac{n\,k\,T}{\frac{B^2}{\mu_0}} \ . \tag{3.6}$$

Lowest β-values are found in the tail lobes, where the mean particle number density is only about $0.03\,\mathrm{cm}^{-3}$ and below. While the temperature in the lobes is high, it holds an extremely good vacuum of $10^{-10}\,\mathrm{Pa}$ (UHV).
The intermediate range of β is in between 0.25 and 2. Such values can be found in the **plasma sheet boundary layer (PSBL)**, the outer part of the central plasma sheet. Here the density is about 10 times higher $0.3\,\mathrm{cm}^{-3}$, with an ion temperature of $\sim 4.2\,\mathrm{keV}$ and an electron temperature of $\sim 0.6\mathrm{keV}$.
High β-values $\beta > 2$ indicate the innermost part of the plasma sheet. When the magnetic field is simultaneously weakest, nearly zero, we're in the current sheet.

The **plasma mantle** is the outermost part of the geomagnetic tail. The mantle plasma population originates from 2 different sources

- the magnetosheath,

- the ionosphere.

It was previously described that the magnetopause is a closed boundary and no plasma or magnetic field can cross it. This is only true as long as the frozen-in flux concept holds. When this concept is violated and breaks down we find reconnection that allows plasma and magnetic field to cross this barrier. Under special circumstances, when reconnection occurs, plasma from the magnetosheath can enter the plasmasphere on the day side. This process is called dayside reconnection.
The magnetosheath plasma is guided along magnetic field lines toward the poles, forming the *dayside cusp population*, where the magnetic field strength increases. Due to the mirror effect, it is reflected back and leaves this region called cusp to

be finally part of the plasma mantel. This plasma is relatively warm, $\sim 300\,\text{eV}$ consisting mainly of H^+ and He^{++}, compared to the mantles second plasma source, the ionosphere. Ionospheric plasma is of only a few eV in temperature and consists of O^+, He^+ and H^+.

As there is a magnetic field gradient in the lobes the mantle plasma is convected along decreasing field strength toward the center plane while flowing down the tail. At the center plane or current sheet the **x-line** is the second locus that allows reconnection to take place. The incoming plasma is accelerated during reconnection and forms the *plasma sheet population.*

Tail reconnection has more symmetric plasma inflow than day side reconnection. From the north and south lobe incoming plasma has similar properties. Only the outflow regions are different.
Earthward of the x-line the outflowing plasma is put on closed flux tubes. After acceleration it moves fast to the north or south pole where it is reflected (mirror effect) and bounces from hemisphere to hemisphere. Counterstreaming particles thermalize each other after a few bounces and end up in isotropic plasma.
Compared to tailward accelerated plasma, it is denser and slower moving.
Particles that are accelerated away from Earth move along purely interplanetary magnetic field lines and ultimately rejoin the solar wind. So the outflow region is split into earthward directed planetary and tailward directed purely interplanetary flux tubes.
Depending on their energy particles escape tailward or are retained on the earthward side.

3.1.3 Plasmasphere and Ionosphere

The inner part of the magnetosphere is rather symmetrically built around the Earth's surface. There are many different and partly overlapping layers with different regimes of particles.

The **ionosphere** is a part of the atmosphere, starting above the stratosphere, where ultaviolett light and x-ray ionize atmospheric molecules. It ranges from about 50 up to 500 km. Depending on it's radio wave propagation property it is divided into D, E, and F layer. The *topside ionosphere* reaches out to a few 1000 km and feeds at mid-latitudes into the **plasmasphere** [DDi].

The **plasmasphere** arises from the ionosphere at altitudes, where the density is low enough to support and sustain a plasma, which is true for about 90 km above ground. The *plasmaspheric population* is dense and relatively cold of only $\sim$2000 K. It has a donut-like shape starting at the inner radiation belt with its outer limit at up to $\sim 4\,R_E$ or 25 000 km, the *plasmapause* [DDp]. The plasmasphere is not static. Its shape and size are strongly dependent on space weather conditions. Increasing space weather activity shrinks and distorts (plasmaspheric erosion) the plasmasphere, while during inactivity it can refill to equilibrium size.

The two radiation belts around the Earth are the **Van Allen belts**. Each has a torus shape but inner and outer Van Allen belt don't adhere the same

kinds of particles. While the outer belt consists of energetic electrons coming from the solar wind mainly, the inner belt is composed of protons and electrons from both, solar wind and ionosphere. Apart from that both belts contain lesser amounts of other nuclei like α-particles.
The belts are closely related to the aurora-phenomenon.
The outer belt can be found at 3-10 R_E with its maximum at 4-5 R_E and the inner belt at 0.01-1.5 R_E [Wik].

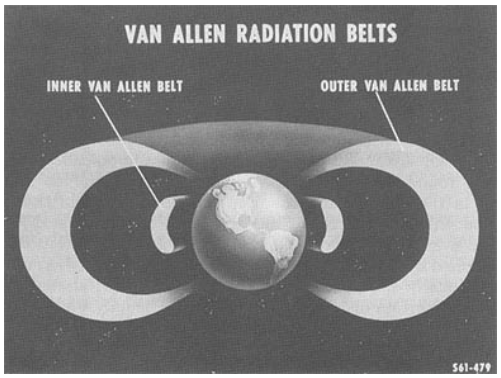

Figure 3.2: Van Allen belts [DDV]

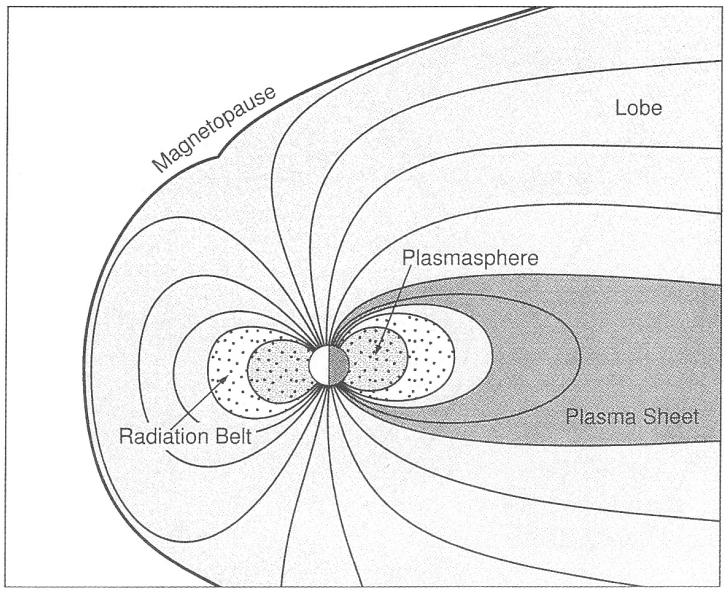

Figure 3.3: Plasmasphere [BT96]

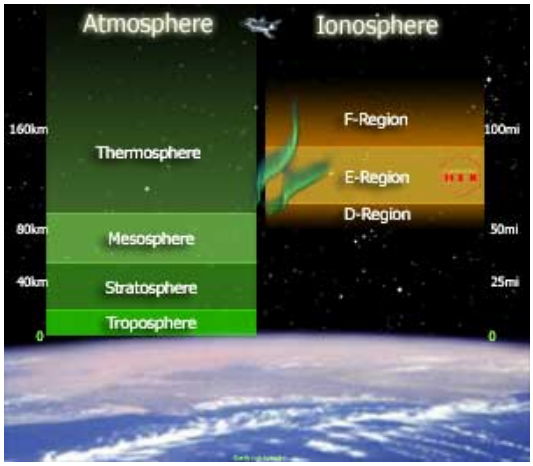

Figure 3.4: Ionosphere [DDi]

3.2 The Frozen-in Flux Concept

As it was mentioned before the Frozen-in Flux Concept is the reason why solar wind plasma cannot easily enter the magnetosphere and is decelerated and deflected around it instead. This holds except for the case of reconnection when the concept breaks down.
There are 2 possible ways to describe plasma dynamics: the Particle Description and Magnetohydrodynamics. From the particle description some characteristic quantities like gyroradius, gyrofrequency, Debye length or plasma frequency can be derived.
The fluid description or Magnetohydrodynamics describes plasma properties in a locally averaged form. We need a statistically significant particle number, time scales long compared to microscopic particle motion like cyclotron motion or inverse plasma frequency and spatial scales large with respect to Debye length or gyroradius [RK95]. Now we can apply basic conservation laws for energy, mass and momentum.
To derive the Frozen-in Flux Concept, these basic magnetohydrodynamic equations are needed

$$\text{I.} \quad \frac{\partial \rho}{\partial t} + \nabla \cdot (\rho \mathbf{v}) = 0 \qquad \text{continuity equation,} \tag{3.7}$$

$$\text{II.} \quad \mathbf{E} + \mathbf{v} \times \mathbf{B} = \frac{1}{\sigma}\, \mathbf{j} \qquad \text{generalized Ohm's law,} \tag{3.8}$$

$$\text{III.} \quad \nabla \times \mathbf{E} = -\frac{\partial \mathbf{B}}{\partial t} \qquad \text{Faraday's law,} \tag{3.9}$$

$$\text{IV.} \quad \nabla \times \mathbf{B} = \mu_0 \mathbf{j} \qquad \text{Ampère's law in MHD-limit.} \tag{3.10}$$

First step is to calculate the rotation of $\mathbf{E}$ in equation (3.9). With help of equation (3.8) $\mathbf{E}$ is expressed. From equation (3.9) we get the current density $\mathbf{j}$. This leads us to the following equation

$$\nabla \times \mathbf{E} = \frac{1}{\sigma \mu_0} \nabla \times (\nabla \times \mathbf{B}) - \nabla \times (\mathbf{v} \times \mathbf{B}) = -\frac{\partial \mathbf{B}}{\partial t}\ . \tag{3.11}$$

Now the following 2 operator identities are used

$$\nabla \times (\mathbf{v} \times \mathbf{B}) = \mathbf{B} \cdot \nabla \mathbf{v} + \mathbf{v}(\nabla \cdot \mathbf{B}) - \mathbf{v} \cdot \nabla \mathbf{B} - \mathbf{B}(\nabla \cdot \mathbf{v})\ , \tag{3.12}$$

$$\nabla \times (\nabla \times \mathbf{B}) = \nabla(\nabla \cdot \mathbf{B}) - \nabla \cdot \nabla \mathbf{B} = -\Delta \mathbf{B}\ . \tag{3.13}$$

Due to the fact that the magnetic field is divergenceless

$$\nabla \cdot \mathbf{B} = 0\ , \tag{3.14}$$

the right hand side of equation (3.13) becomes equal to the second derivative of $\mathbf{B}$. Our equation (3.11) turns into equation (3.16)

$$\frac{\partial \mathbf{B}}{\partial t} - \nabla \times (\mathbf{v} \times \mathbf{B}) = -\frac{1}{\mu_0 \sigma} \nabla \times (\nabla \times \mathbf{B})\ , \tag{3.15}$$

$$\frac{\partial \mathbf{B}}{\partial t} + \mathbf{v} \cdot \nabla \mathbf{B} + \mathbf{B} \left(\nabla \cdot \mathbf{v} \right) - \left(\mathbf{B} \cdot \nabla \right) \mathbf{v} = -\frac{1}{\sigma \mu_0} \Delta \mathbf{B} \ . \tag{3.16}$$

Now we divide by ρ

$$\frac{1}{\rho} \left(\frac{\partial \mathbf{B}}{\partial t} + \mathbf{v} \cdot \nabla \mathbf{B} \right) + \frac{\mathbf{B}}{\rho} (\nabla \cdot \mathbf{v}) - \frac{\mathbf{B}}{\rho} \cdot \nabla \mathbf{v} = -\frac{1}{\rho} \frac{1}{\sigma \mu_0} \Delta \mathbf{B} \ . \tag{3.17}$$

From the continuity equation we get:

$$\nabla \cdot \mathbf{v} = -\frac{1}{\rho} \left(\frac{\partial \rho}{\partial t} + \mathbf{v} \cdot \nabla \rho \right) \ , \tag{3.18}$$

with which equation (3.17) becomes

$$\frac{1}{\rho} \left(\frac{\partial \mathbf{B}}{\partial t} + \mathbf{v} \cdot \nabla \mathbf{B} \right) - \frac{\mathbf{B}}{\rho^2} \left(\frac{\partial \rho}{\partial t} + \mathbf{v} \cdot \nabla \rho \right) - \frac{\mathbf{B}}{\rho} \cdot \nabla \mathbf{v} = -\frac{1}{\rho} \frac{1}{\sigma \mu_0} \Delta \mathbf{B} \ . \tag{3.19}$$

The first 2 terms can be simplified

$$\frac{\partial}{\partial t} \frac{\mathbf{B}}{\rho} + \mathbf{v} \cdot \nabla \frac{\mathbf{B}}{\rho} = \frac{1}{\rho} \left(\frac{\partial \mathbf{B}}{\partial t} + \mathbf{v} \cdot \nabla \mathbf{B} \right) - \frac{\mathbf{B}}{\rho^2} \left(\frac{\partial \rho}{\partial t} + \mathbf{v} \cdot \nabla \rho \right) \ . \tag{3.20}$$

Our final equation is:

$$\frac{\partial}{\partial t} \frac{\mathbf{B}}{\rho} + \mathbf{v} \cdot \nabla \frac{\mathbf{B}}{\rho} - \frac{\mathbf{B}}{\rho} \cdot \nabla \mathbf{v} = -\frac{1}{\rho} \frac{1}{\sigma \mu_0} \Delta \mathbf{B} \ . \tag{3.21}$$

There are basically 2 possible cases:

a) in ideal plasma conductivity is infinite, $\sigma = \infty$, and the right hand side becomes zero,

$$\frac{\partial}{\partial t} \frac{\mathbf{B}}{\rho} + \mathbf{v} \cdot \nabla \frac{\mathbf{B}}{\rho} - \frac{\mathbf{B}}{\rho} \cdot \nabla \mathbf{v} = 0 \ .$$

The left-hand side of equation (3.21) is the Lie derivation of fields $\dfrac{\mathbf{B}}{\rho}$ and $\mathbf{v}$. As it vanishes the field $\dfrac{\mathbf{B}}{\rho}$ is frozen into the plasma velocity $\mathbf{v}$. We interpret this as magnetic field lines being convected with the plasma flow itself. After some time plasma still finds itself on the same magnetic field line as before. Therefore as the flow cross section area widens and narrows the number of field lines it is pervaded with is constant,

$$\Phi = \int \mathbf{B} \ \mathrm{dS} \ . \tag{3.22}$$

The total magnetic flux Φ crossing the surface S remains constant. If S shrinks or stretches, magnetic field lines move closer or apart and respectively the field weakens or strengthens.

A flux tube is a spatial volume where Φ is constant along any cross section within it. Equation (3.8) can also be used as frozen-in flux condition if its right side is zero,

$$\mathbf{E} + \mathbf{v} \times \mathbf{B} = 0 \qquad \text{frozen-in flux condition.} \tag{3.23}$$

As a consequence all particles initially on a flux tube remain linked as they convect.

Actually plasma moves along magnetic field lines, but in the frozen-in flux concept field lines can be thought of as moving with the plasma flow. This behavior is well known from fluid mechanics.
There is the notion of vortex line and vortex field in a frictionless fluid which fulfills the following equation

$$\mathbf{w} = \nabla \times \mathbf{v} \ . \tag{3.24}$$

This is analogous to the frozen-in flux condition (eqn. 3.23).
Concerning an ideal plasma ($\sigma \to \infty$) the next equation is in analogy to equation (3.15), as its right-hand side becomes zero

$$\frac{\partial \mathbf{w}}{\partial t} - \nabla \times (\mathbf{v} \times \mathbf{w}) = 0 \ . \tag{3.25}$$

This provides the chance to use all theorems that are true for hydrodynamics to be true for ideal plasma as well. One of these is that vorticity is propagated by the flow and that vortex tubes are characterized by the same masspoints moving with the flow. In MHD we call this flux tube $\mathbf{w} = \frac{\xi}{\rho}$.

b) For non-ideal plasma the conductivity is finite.

The frozen-in flux concept leads to large uniform regions of plasma, separated from neighboring regions by thin current sheets such as the magnetopause or the neutral sheet in the magnetotail. Different plasma populations and magnetic fields cannot mix easily. Hence the solar wind cannot enter the magnetosphere except if the condition breaks down, which is true for reconnection.

Actually equation (3.8) is just an approximation. To describe processes in the magnetosphere and outside of it further terms might be important. If there is a current, $\mathbf{j} \times \mathbf{B}$ causes the Hall effect, which is small in this regions. In the ionosphere and plasmasheet sufficient currents are expected, and we do not neglect it. Perpendicular to the magnetic field there should be no current.

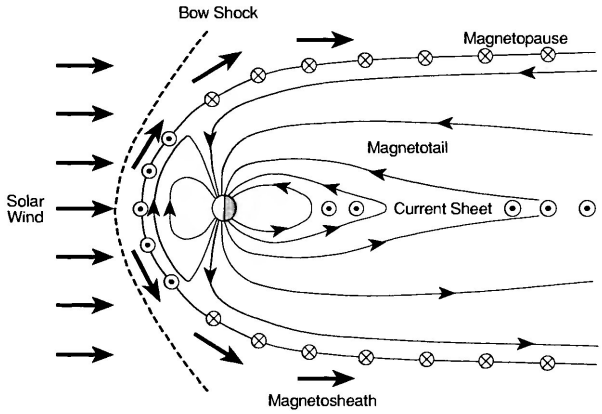

Figure 3.5: Closed magnetosphere. Solar wind cannot enter it and is deflected around it instead, [RK95].

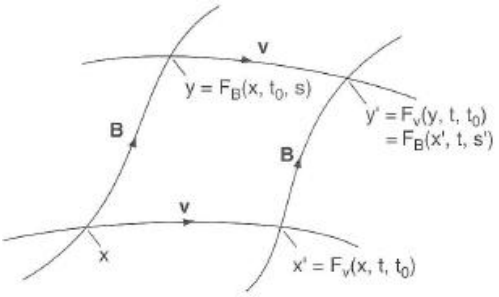

Figure 3.6: Magnetic field line frozen into plasma flux of velocity $\mathbf{v}$ for time t_0 and time $t_1 > t_0$ [BP07].

3.3 Reconnection

3.3.1 Basic x-line picture

The concept of reconnection was first proposed to explain rapid plasma heating in solar flares. Its more profound effect is probably that, due to the violation of the frozen-in flux concept, plasma from different sources can mix when crossing current sheet boundaries like the magnetopause or the neutral sheet in the magnetotail.

A direct consequence of the frozen-in flux concept are thin current sheets that separate regions of different magnetic fields and plasma regimes. In equation (3.8) we used a simple form of generalized Ohm's law. The complete formula is this

$$\text{II.} \qquad \mathbf{E} + \mathbf{v} \times \mathbf{B} = \frac{1}{\sigma}\,\mathbf{j} + \frac{1}{ne}\mathbf{j} \times \mathbf{B} - \frac{1}{ne}\nabla \cdot \mathbf{P}_e + \frac{m_e}{ne^2}\frac{\partial \mathbf{j}}{\partial t}\ . \tag{3.26}$$

This more complicated form contains not only the resistive term $\frac{1}{\sigma}\mathbf{j}$, but addi-

tional the Lorentz force or Hall term $\mathbf{j} \times \mathbf{B}$, an electron-pressure term and a time variation of the current density $\mathbf{j}$. It can be derived from momentum equation of electrons and ions.
For weak currents, slow variations and vanishing pressure gradient these additional terms can be neglected and the simple form of equation (3.8) can be used, which was the case before.
When it comes to current sheets, where sufficient currents occur, these terms become important and the frozen-in flux concept breaks down.

First one thought that magnetic flux, for example in the lobes of the magnetotail, diffuses down the field gradient towards the current sheet, where it annihilates with oppositely directed magnetic flux from the other side of the plane carried by plasma. The problem in this picture is, that there is only plasma inflow, but no outflow. To solve this problem we reduce the plane of annihilation in between the different regions to a single line the so called x-line. Now the magnetic field is not zero across the whole plane that separates the regions, but only along this single x-type neutral line. For a steady state ($\frac{\partial}{\partial t} = 0$) a spatially uniform $\mathbf{E}_y$ is needed

$$-\nabla \times \mathbf{E} = \frac{\partial \mathbf{B}}{\partial t} = 0 \qquad \text{Faraday's law,} \tag{3.27}$$

for the x-component

$$\frac{\partial E_y}{\partial z} = 0 \ . \tag{3.28}$$

This field drives flow inward from top and bottom and outward perpendicular to it. Around the x-line there is a small region called the diffusion region (DR). Here scales are small and MHD breaks down locally. Instead of being annihilated, magnetic field lines enter this region from top and bottom, are cut and reconnected to new partners from the opposite side of the plane and finally leave to both sides. A consequence of this is that plasma originating from former– due to the frozen-in-flux concept– separated regions, is being mixed as it is found on a totally new type of flux tube. This is an open boundary with a finite normal magnetic field component. Plasma can cross it by simply following flux tubes.

Even though the diffusion region is very small, the process affects the whole new flux tubes and therefore the entire regions it connects.

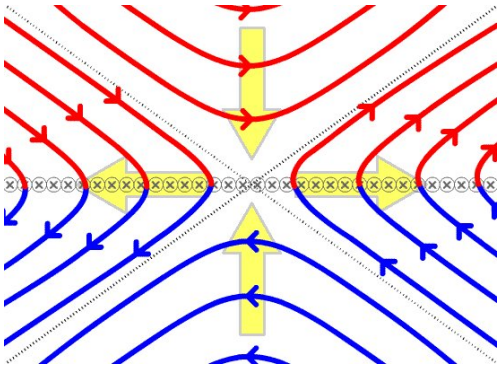

Figure 3.7: Reconnection of 2 oppositely directed magnetic fields, blue and red [rec].

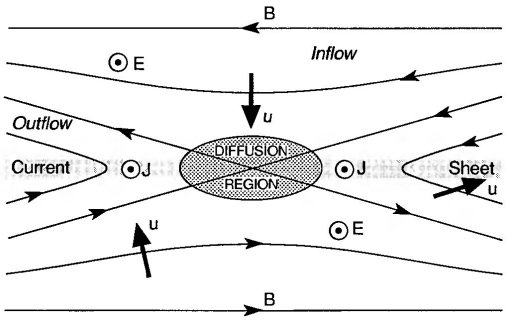

Figure 3.8: Basic x-line picture [RK95].

3.3.2 Fluid description of reconnection

As it was mentioned there are 2 possible ways to describe reconnection

- fluid description,
- kinetic description.

At first there was the classical approach of 2 dimensional reconnection via MHD. Unfortunately this approach had multiple deficiencies like the particle heating mechanism, the breaking condition for the frozen-in flux concept and the onset problem, and had to be further improved several times. Let's go back to the beginning.

The term of reconnection was introduced by Dungey in 1953. He was interested in the processes that lead to particle acceleration in the Earth's magnetosphere [BP07]. With an MHD-approach he introduced thin current sheets where diffusion of magnetic flux takes place. Magnetic field lines are cut and change connectivity to one another. He called this process *disconnection* followed by *reconnection*.

Sweet-Parker model

A few years later Sweet (1958) and Parker (1957) developed a quantitative model for steady-state reconnection in 2 dimensions for an incompressible plasma. Reconnection of course occurs in the current sheet, which was thought to be of global scale length.
The problem that occurred in this picture was the low inflow speed and accordingly the small reconnection rate, much to low for processes in solar flares to take place. Instead of the few minutes of observation time they would take tens of days to grow. The model needed to be improved.

The inflow speed can be determined by the following equation

$$v_i = v_A \frac{1}{\sqrt{S}} \qquad \sim \frac{\delta}{\Delta} v_A \ , \tag{3.29}$$

v_i... inflow speed,
v_A... Alfvén speed.

$S = \mu_0 L \sigma v_A$ is the *Lundquist number* and L the global sale length of the current sheet. Often S is referred to as the *magnetic Reynold's number* R_m. In astrophysical and space plasmas S is very large ($S \gg 10^6$) and the inflow speed becomes very slow. The outflow speed is the Alfvén speed v_A. A quantitative measure of the reconnection rate is the *Alfvén Mach number*, the ratio of inflow to outflow speed. It prescribes the rate at which magnetic flux changes the topological domain. In the Sweet-Parker model the rate becomes

$$M_A = \frac{v_i}{v_A} = \quad \frac{1}{\sqrt{S}} \ , \tag{3.30}$$

hence very low.

The approximation on the right-hand side of equation (3.29) shows that if the ratio of width δ by length $L = \Delta$ of the current sheet, as the site of reconnection, wasn't so small, the inflow speed would increase dramatically. This is exactly what the next model is about.

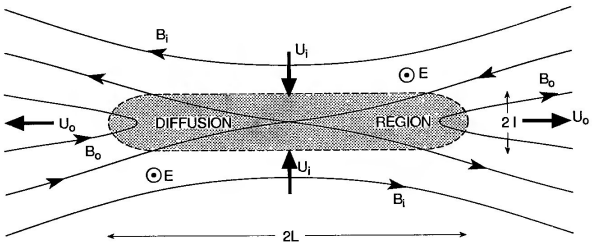

Figure 3.9: Sweet-Parker model of reconnection [RK95]. $L \gg l$

Petschek model

In 1964 Petschek proposed a model with increased reconnection rate associated with a reduced length of the current sheet respectively the region of reconnection, the diffusion region. He did this by encasing it in an exterior field with

global scale length L and also introduced 2 pairs of standing slow-mode shocks [BP07]. The diffusion region is reduced to a dot in the center. Emanating from it are 4 shock waves, where an abrupt change takes place

- magnetic field strength decreases,
- magnetic flow speed increases,
- and the normal component of the flow velocity drops.

The slow-mode shock waves are current sheets at the same time, needed to change magnetic field and flow speed by the Lorentz force term $\mathbf{j} \times \mathbf{B}$. Thus most plasma does not need to pass the diffusion region to be accelerated. It passes through the shock waves instead, where it is accelerated in the so called convection region, where MHD is still valid. This increases the inflow speed significantly. Also this is an energy conversion from magnetic energy to acceleration and heating of plasma and produces two hot outflow jets.

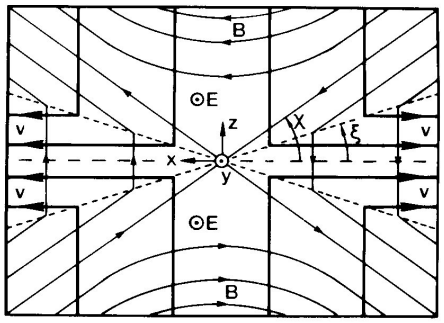

Figure 3.10: Petschek model [RK95]. Dashed lines are shock waves. Outflow is accelerated at shock waves, apparent in narrowing field lines, while magnetic field lines are further apart in the outflow region leading to a decrease in field strength.

Sonnerup

Sonnerup (1970) introduced a further set of shock waves that compress both the magnetic field and plasma in the inflow region. These shocks are fast-mode shock waves that divert the flow direction. This process is completed at the slow-mode shocks where the largest increase of flow speed occurs [RK95]. External boundary conditions define the location of the fast mode shocks. This model further increases the limit of the maximum inflow speed found in Petscheks solution.

Forbes and Priest

Forbes and Priest (1986, 1987) found a general solution. It includes Petschek's as well as Sonnerup's solutions as special cases governed by boundary conditions. Reconnection becomes a more macroscopic problem as external conditions influence it. They were generalized and a family of solutions was found.

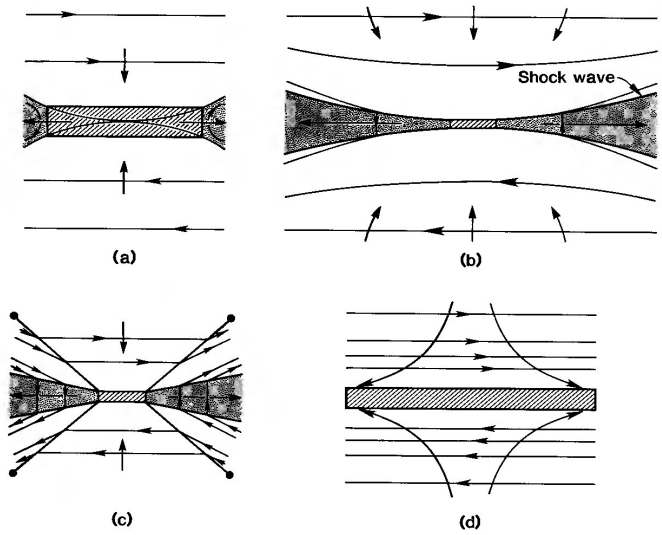

Figure 3.11: Comparison of models: (a) is the Sweet-Parker model, (b) Petschek introduced slow mode shocks, (c) Sonnerups model includes additional a set of fast mode shocks. In (d) Sonnerup and Priest showed the effect of reconnection to the flow. [RK95]

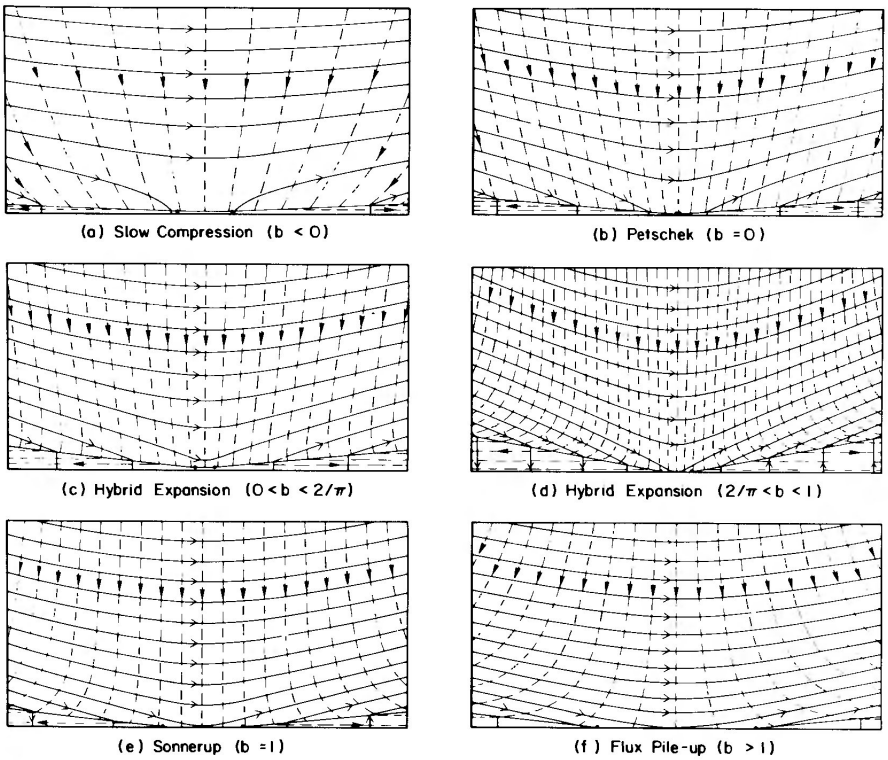

Figure 3.12: Different boundary conditions, indicated by parameter b, of Forbes' and Priest's unifying model. Dashed lines are streamlines, solid lines are magnetic field lines. [RK95] From Forbes and Priest (1986)

3.4 Where does Reconnection occur?

What was first observed and measured concerning magnetospheric flows in the atmosphere was a double-vortex flow pattern, which transports plasma from noon toward midnight over the polar region and back to the day side at lower latitudes near the auroral zone. This cycle is found on both the dusk and dawn side and is stationary at sun fixed coordinates. Due to its similarity with the flow in a raindrop driven by the air surrounding it, it was called **convection** and this was also the first explanation with the solar wind corresponding to the external force of the air.

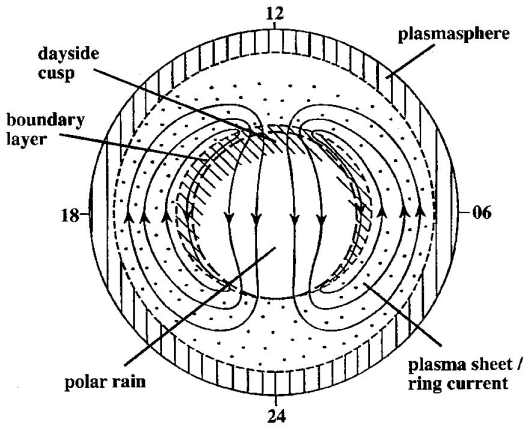

Figure 3.13: Double-vortex flow pattern of convection [ST98].

Dungey 1961 proposed an alternative explanation. A reconnection site at the magnetopause sunward of the Earth. Suppose the interplanetary magnetic field is predominantly southward, while the magnetic field inside the magnetosphere is directed from south to north. These antiparallel fields form an x-line giving rise to reconnection. The IMF-field lines and the purely magnetospheric field lines are cut and reconnected and two open field lines form. Each connected to the Earth at one end and stretching out into space at the other. An electric field is sensed all along these flux tubes.

$$\mathbf{E} = \mathbf{v}_{\mathrm{SW}} \times \mathbf{B}_{\mathrm{SW}} \qquad \mathrm{SW} \ldots \text{solar wind} \tag{3.31}$$

At the ionosphere the field is directed from dawn to dusk and drives the flow and field lines from noon toward midnight. Subsequently the field lines are drawn out to form the geotail and would end up somewhere in the solar wind flow if there wasn't any process to close the field lines. This actually happens at a second reconnection site in the geotail, the neutral line. An open field line from the southern hemisphere reconnects with another open field line from the northern lobe and again two new field lines are formed. One is the required closed field line that keeps the magnetic flux and plasma in the geomagnetic field and directs it back on either the dusk or dawn side at lower latitude to the day side. The other field line is purely interplanetary and ends up as part of

the solar wind.
This yields as well the observed flow pattern but is of course not a steady process. Reconnection rates at the day side magnetopause and the neutral line in the geotail would have to be instantaneously equal, but they rarely are.

Fairfield and Cahill (1966) showed that the magnetospheric activity is modulated by the north and south component of the IMF.

Dungey's hypothesis is the basis for all following descriptions of magnetospheric physics and shows the importance of reconnection to the dynamics and transport in (and outside) the magnetosphere.

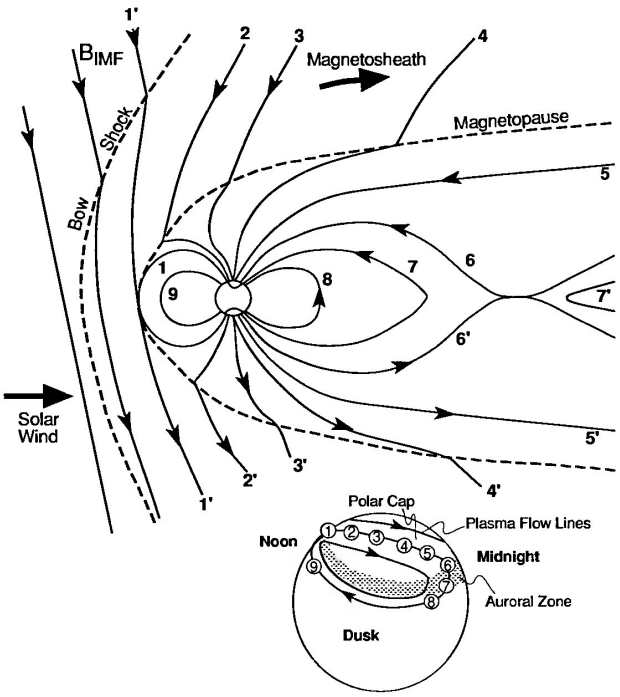

Figure 3.14: Model of Convection [RK95]. Flow pattern as observed from the Earth and its corresponding field lines moving through numbered regions across the magnetosphere. Reconnection occurs at the front of the magnetosphere, connecting the IMF-line 1′ and the planetary field line 1, and in the tail connecting 6′ and 6, both planetary field lines.

3.5 Magnetospheric Substorms

The processes in the magnetosphere as described before are not in a steady state. Its time evolution is called **magnetospheric substorm**.
The evolution is modulated by the IMF on a 1-2 hour time scale. First the magnetosphere is in a ground state as the IMF is directed northward. The substorm is initiated with an IMF southward turn, which activates day side reconnection. The day side reconnection rate is the amount of magnetic flux merged per unit

time. It depends on the number of southward oriented interplanetary field lines in contact with the magnetopause and thus on the solar wind velocity. In quiet periods the IMF is predominantly northward oriented and convection ceases.
The reconnection rates at magnetopause and in the tail need to be equal, but only on average not instantaneously. At this point in time the distant x-line in the tail is relatively inactive with little or no reconnection activity.
The day side magnetopause moves in toward Earth up to $1\,R_E$. Flux eroded there is transported into the magnetospheric tail, where radius and field strength increase. Only part of the flux is reconnected and convected back to the front side immediately. The not jet reconnected part of the flux is added to the tail lobes and leads to a growth of magnetic field strength, which is accompanied by growing current in the current sheet, according to Biot-Savart's law. Field lines are stretched and the plasma sheet receives a more tail like form.
This is the **initial growth phase**, which lasts about some tens of minutes. The current in the near-Earth current sheet ($\sim 10R_E$) becomes concentrated in a 500-1000 km thin layer -in ground state about 300 000 km- and develops in intensity.
When too much magnetic flux and energy is accumulated in the tail, it becomes unstable. This is the **substorm onset** and the beginning of the **Expansion phase**. A new neutral line is formed, where plasma is compressed and heated. At a distance up to $30\,R_E$ it is called near-Earth neutral line (NENL), while the distant neutral line (DNL) is situated at 100-200 R_E downwards. The large region between these two neutral lines is a topologically new structure, the *PLASMOID*. Its field lines are neither terrestrial nor interplanetary. Either they form closed loops or, if the magnetic field inside has a dawn-dusk component, a 3 dimensional helix. At the top of the atmosphere a sudden and intense flux, the aurora phenomenon is triggered. The expansion phase lasts about 30 to 60 minutes.
When ionospheric currents start do decrease and the near-Earth reconnection ceases the substorm activity settles and the **recovery phase** begins. The near-Earth neutral line moves down the tail and finally becomes the distant neutral line. The plasmoid moving down the tail finally is ejected and rejoins the solar wind at a speed between 400 and 800 km/h. This recovery process takes 1-2 hours and ends when the magnetosphere is in a quiet state.

If the southward IMF persists longer than a few minutes the whole system evolves through a series of substorm cycles, each about one hour. Together they show the main characteristics of a magnetic storm, for example the worldwide decrease of magnetic field strength on the ground.

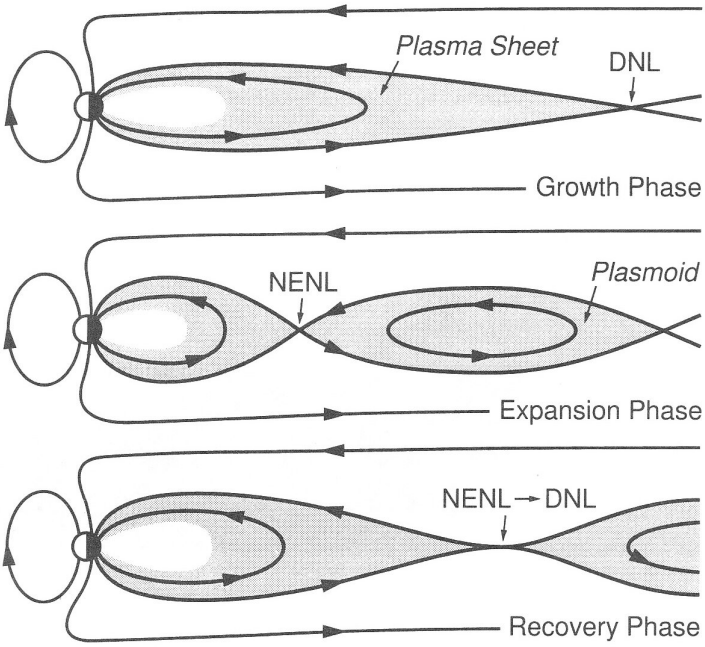

Figure 3.15: Phases of magnetospheric substorms [BT96].

Chapter 4

Data Analysis

In this chapter we will see how Cluster Mission data is used to find out more about reconnection in the near-Earth magnetotail. The objective of this study is to perform a search on a certain amount of data, distinguish between useful and less useful results, optimize search criteria and use best results for statistics to find out more about profound physical basics.

4.1 Data

First let's have a look at data and the way it is measured and processed. There are 3 datasets being used:

- AUX
- FGM
- CIS

Cluster Active Archive

Data can be downloaded by every scientist from **Cluster Active Archive** (CAA) after registration. The Cluster Active Archive is a depository of processed and validated high-resolution Cluster data, raw data, processing software, calibration data, documentation and other value added products [CAA].
It also provides a set of services like advanced search, data visualization, holds support information and documentation. The data visualization tool, the graphical product on the website, will be used in this thesis as well.
From October 2001 on exists one file per day and dataset available in CDF format (Common Data Format) as well as CEF (Cluster Exchange Format). The CEF-format is intended to be used for exchange of science data between instrument teams. CDF format is a product by NASA/Goddard Space Flight Center and is free to all users. CDF is a scientific data management product.

In table 4.1 are examples of filenames. These are the filenames of July 1st 2001. Auxiliary-data includes information on all 4 Cluster-spacecraft and the filename starts with CL. FGM and CIS datasets are in separate files for each spacecraft and the filename starts with C and the number of the spacecraft. The last term stands for the version of the dataset. A higher version number means

dataset	filename	sampling rate
AUX	`CL_SP_AUX_20010701_V02.cdf`	1 min
FGM	`C1_PP_FGM_20010701_V01.cdf`	4 sec
CIS	`C1_PP_CIS_20010701_V03.cdf`	4 sec

Table 4.1: Overview of downloaded datasets, their filenames and sampling rates

that the data was reprocessed and improved several times. In data-analysis the highest available version was used. The currently latest possible version is V03.

In this thesis the software used to perform data analysis is MATLAB. To read data stored in a CDF file the Patch **cdfread** was used. This patch can be downloaded for free from NASA's web page `http://cdf.gsfc.nasa.gov/html/matlab_cdf_patch3.html`, where a short manual can be found as well. It converts the dataset into a MATLAB-structure, with field names referring to its data-vector content stored in cells.

4.1.1 Auxiliary Data AUX

Auxiliary data contains information about the spacecraft position. Data is taken by Cluster on a one minute time base. The absolute position refers to a reference spacecraft, which is spacecraft Cluster 3. Specification about Cluster 1, 2 and 4 is given in relative distance to Cluster 3. The file also contains metadata.

Coordinate Systems

The position data in AUX-data-files is given in GSE coordinates.

Geocentric Solar Ecliptic System GSE is short for geocentric solar ecliptic system. In this coordinate system the x-axis is pointing from Earth towards the Sun. The z-axis is chosen to be perpendicular to the ecliptic plane, in the same sense as the ecliptic north pole. The y-axis, perpendicular to both and completing the right-hand coordinate system, points in the ecliptic plane from dawn to dusk. The system has an annual rotation about the sun, compared to an inertial system.
It is used for interplanetary magnetic field observations, displaying satellite trajectories and solar wind velocity measurements.

As we are mainly inside the magnetosphere collecting data, we need a coordinate system better attached to the Earth itself.

Geocentric Solar Magnetospheric System This Coordinate system, short GSM, is much more suitable for measurements inside the magnetosphere.
The x-axis is directed towards the sun in the same sense as in GSE. The y-axis is perpendicular to the magnetic dipole axis, hence in the magnetic equator also pointing towards dusk. The x-z-plain contains the dipole axis. The z-axis is the projection of the dipole axis on a plane perpendicular to x.

It is used for all components of the magnetosphere like magnetopause, magnetosheath, magnetotail and also to determine the positions of shock waves like

the bow shock.

Therefore AUX-data was recalculated to GSM coordinates. This was done using the function `GEOPACK_GSMGSE`. The transformation matrix is of the following form :

$$\begin{pmatrix} 1 & 0 & 0 \\ 0 & cos\theta & -sin\theta \\ 0 & sin\theta & cos\theta \end{pmatrix}$$

GSE and GSM mainly differ in the alignment of their z-axis. The GSE coordinate system rotates about the sun, while its z-axis is constant in space. GSM coordinate system also rotates about the sun each year in the same way, but its z-axis is not constant in space. The difference between the systems is a rotation about the x-axis. θ is the tilt angle between the 2 z-axis'. This angle cannot easily be deduced because it is dependent on both, an annual and a diurnal variation. To transform from GSE to GSM the exact date is needed.

The function `GEOPACK_GSMGSE` can recalculate the coordinates not only from GSM to GSE but also from GSE to GSM.

```
[X,Y,Z]=GEOPACK_GSMGSE(x,y,z,j)
```

The variables x, y and z are coordinates or vectors of coordinates in either of the systems.
j determines the direction of the transformation. It has to be $+1$ in case of transformation from GSM to GSE or -1 for GSE to GSM.

GSE$\rightarrow$ GSM : j= -1
GSM$\rightarrow$ GSE : j= $+1$

After transformation to GSM-coordinates, the unit was changed from km to Earth radii R_E. Because the distances are large, this unit is more useful in this context. It is a simple division by $R_E = 6380\,\text{km}$. This is not the exact value, in particular because of the ellipsoidal shape, but for this purpose sufficiently accurate. To go back to the exact value we simply multiply by this value.

$R_E = 6380\,\text{km}$

The auxiliary data file contains the complete orbits. To analyze reconnection in the near magnetotail, the orbit data apart from the tail is needless. So we cut it out. The criterion for keeping useful orbit data is

$x < -8\,R_E$.

Auxiliary data is taken on a one-minute time base. This resolution is relatively low, compared to other datasets, but by far high enough, as it is a slowly varying parameter.

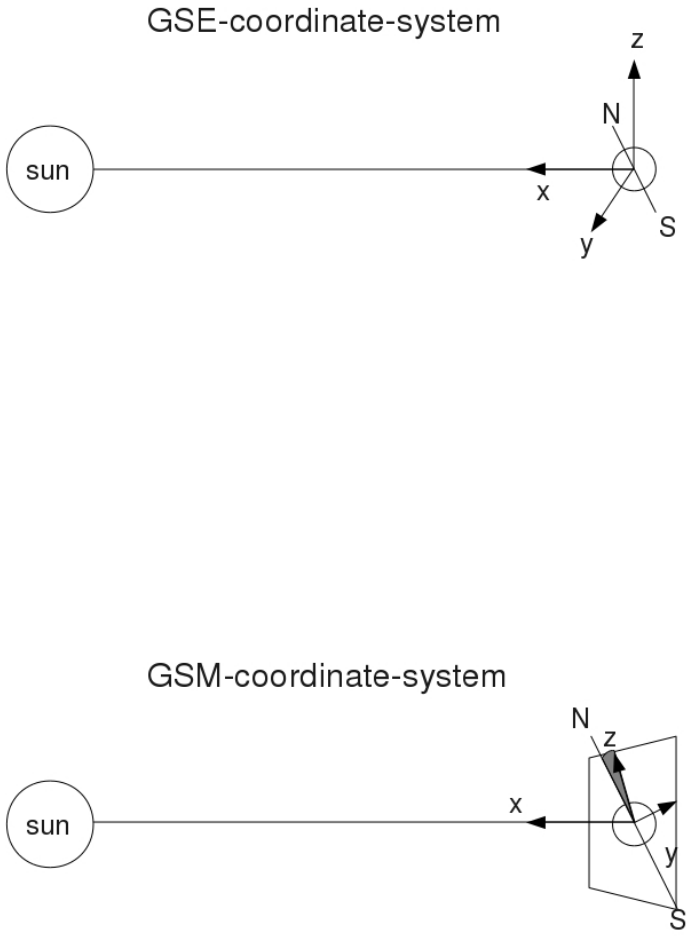

Figure 4.1: Coordinate systems

$\Delta t = 1\,min$

In the function `autoAUX.m` these calculations are performed. The CDF-data files are loaded for each day of one month and one spacecraft, processed and a MATLAB-structure is generated. The structure array is of the following size:

`1 x days_of_month`:	`1 x 31`	...July, August, October
	`1 x 30`	...September

Each day of month is stored in one structure-element with its index corresponding to the number of day. The structure elements contain 1- or more-dimensional arrays, as values in the following fields:

field names:
`Time`
`timenum`
`SC_xyz`

In the `Time`-field a cell array containing date-strings of the original dataset can be found, given in universal time, UT.
Via the MATLAB-function `datenum` a datestring, a datevector or an array of either of these can be converted to a serial date number. This was done to produce the field `timenum`. Of course these two fields are redundant but in this case it was done for safety issues, only for this one dataset and abandoned in all further. If the datenum-function was not available for any reason anymore the comparison of these fields could replace it.
The last field's value, `SC_xyz`, is the position of the spacecraft in GSM coordinates. It is a 3-dimensional vector of x, y and z coordinate-values in its columns. The number of row corresponds to the same row in the row-vector of the `timenum`-value. Therefore it is very important that the rownumber as well as the total number of rows matches.

`N = datenum(M)`	MATLAB-function; M is a string- or a $n \times 6$-vector
`str(9).timenum`	calls the vector of timenumbers of day 9 of month

The structure can only be stored as `1x1 struct`. It is stored in a MATLAB-data-file with the file name composed of AUX, the number of the year, the name of the month and to distinguish between spacecraft, SC and the number of it. For September 2002 and spacecraft 3 it is:

`AUX2002septemberSC3`

4.1.2 Fluxgate Magnetometer Data FGM

The Fluxgate Magnetometer provides measurement of the magnetic field. On each spacecraft are two tri-axial fluxgate magnetometers with an on-board data-processing unit. Magnetometer sensors are mounted at the tip and, to minimize magnetic field interference from the spacecraft, inwards at 1.5 m of a 5 m radial boom. This architecture is highly fault-tolerant. Besides a high vector sample rate (up to 67 vectors per second) and even a high resolution (up to 8 pT) can be achieved.

Concerning the time-resolution a 4 second dataset was used. This is of course not the same resolution as in auxiliary-data. So the first step was to resample the datasets. The method used was one-dimensional linear interpolation.
This yields very good results because the spacecraft-position is a non-fluctuating continuous and slowly varying parameter. The integrated MATLAB-function `interp1` was applied.

```
YI =interp1(X,Y,XI)
```

The AUX-dataset time is the input variable X and AUX-data position is Y. In XI the demanded new time data-values are inserted, hence the time-data of the FGM-dataset. The function's output are the newly calculated position-values corresponding to FGM-time and resolution. The original FGM-dataset values of the magnetic field are stored in GSE-coordinates. To adjust to GSM-coordinate system, the data is transformed in the same way as before (see 4.1.1).

Also we calculated the new variable `B_tot`, the total magnetic field:

$$B_{tot} = \sqrt{B_x^2 + B_y^2 + B_z^2} \tag{4.1}$$

All recalculated and new variables and values were stored in another structure, built in the same way as before with these field names:

field names:
`FGM_t`
`FGM_xyz`
`B_xyz`
`B_tot`

The field `FGM_t` is the time-data of the original FGM-dataset converted to a datenumber. `FGM_xyz` is a 3-dimensional vector of the same length, in its 3 columns the coordinate position value of x, y and z coordinate.
`B_xyz` is the 3-dimensional vector of magnetic field measurements in nT.
The structure is stored in a MATLAB-data file, named similar to the auxiliary-data structure:

```
FGM2003juliSC4
```

This is the data file of July 2003 of spacecraft 4. There is no overwriting of an auxiliary-data file.

4.1.3 Cluster Ion Spectrometry CIS

The Cluster Ion Spectrometry or Comprehensive Ion Spectrometry provides plasma data.
Full 3-dimensional ion distributions are obtained in this experiment, which consists of two distinct instruments. The Hot Ion Analyzer, HIA, and the COmprehensive DIstribution Function analyzer, CODIF. Together they cover the full range of particle distributions of interest. The HIA is useful for measurement of particle beams, such as the solar wind, while CODIF shows the distribution of major ions like H^+, He^+, He^{++} and O^+ at a range of 0.02 to 40 keV/e. Also

other parameters are calculated by an on-board data-processing unit. All measurements provide good time resolution of one spacecraft spin, which equates to 4 seconds.
Here we use data processed and measured from CODIF. Energy, velocity-vector **V**, angles and counts are measured. Taking these the on-board processed moments are approximated by sums over the distribution function instead of integrals. Particle density N_i , six components of the momentum flux tensor and the heat flux vector are gained. The table shows an overview of moments.

To within a multiplicative factor dependent on the analyser geometric factor, the moments are given by the following sums:

Density:

$$N = \sum_E 1/V(E) \times \sum_\phi \sum_\theta C(\theta, \phi, E)$$

Bulk Velocity:

$$NV_x = \sum_E \sum_\phi \cos(\phi) \times \sum_\theta \cos(\theta) \times C(\theta, \phi, E)$$

$$NV_y = \sum_E \sum_\phi \sin(\phi) \times \sum_\theta \cos(\theta) \times C(\theta, \phi, E)$$

$$NV_z = \sum_E \sum_\phi \sum_\theta \sin(\theta) \times C(\theta, \phi, E)$$

Heat Flux Vector:

$$NH_x = \sum_E V^2(E) \times \sum_\phi \cos(\phi) \times \sum_\theta \cos(\theta) \times C(\theta, \phi, E)$$

$$NH_y = \sum_E V^2(E) \times \sum(\phi)\sin(\phi) \times \sum_\theta \cos(\theta) \times C(\theta, \phi, E)$$

$$NH_z = \sum_E V^2(E) \times \sum_\phi \sum_\theta \sin(\theta) \times C(\theta, \phi, E)$$

Pressure Tensor:

$$NP_{xx} = \sum_E V(E) \times \sum_\phi \cos^2(\phi) \times \sum_\theta \cos^2(\theta) \times C(\theta, \phi, E)$$

$$NP_{yy} = \sum_E V(E) \times \sum_\phi \sin^2(\phi) \times \sum_\theta \cos^2(\theta) \times C(\theta, \phi, E)$$

$$NP_{zz} = \sum_E V(E) \times \sum_\phi \sum_\theta \sin^2(\theta) \times C(\theta, \phi, E)$$

$$NP_{xy} = \sum_E V(E) \times \sum_\phi \cos(\phi) \times \sin(\phi) \times \sum_\theta \cos^2(\theta) \times C(\theta, \phi, E)$$

$$NP_{xz} = \sum_E V(E) \times \sum_\phi \cos(\phi) \times \sum_\theta \cos(\theta) \times \sin(\theta) \times C(\theta, \phi, E)$$

$$NP_{yz} = \sum_E V(E) \times \sum(\phi)\sin(\phi) \times \sum_\theta \cos(\theta) \times \sin(\theta) \times C(\theta, \phi, E)$$

where: E is energy

$\vec{V}$ is velocity

Θ, ϕ are the analyzer viewing angles

$C(\theta, \phi, E)$ are the measured counts

Figure 4.2: On board processed moments, [ERS97]

In the next table there are parameters we used, taken from CIS-data:

name	quantity	unit
`t`	time	string
`N_p`	particle density of protons	cm^{-3}
`Vp_xyzGSE`	velocity of protons in GSE-coordinates	km/s
`T_ppar`	temperature of protons parallel	MK
`T_pperp`	temperature of protons perpendicular	MK

Table 4.2: Parameters in CIS-dataset CDF-file. The names are introduced in the program, during execution.

With a sampling rate of 4 seconds the resolution is equal to FGM-data, but the instruments are not synchronized. Again a resampling is necessary. This time a nearest-neighbor interpolation is applied.
As a consequence, the time difference in magnetic field and plasma values is at most ± 2 seconds.
To maintain both, the time of magnetic field measurement and of plasma distribution measurement, both values are saved in separate fields.
The velocity vector $\mathbf{V}$ contains the x, y and z-coordinate in its columns in GSE coordinates. They are transformed to GSM-coordinates also using `GEOPACK_GSMGSE`-function.

Additional some new quantities are calculated in the function `autoCIS.m`.

$$\mathbf{V}_{\parallel} = \frac{\mathbf{V}\cdot\mathbf{B}}{|B|} \tag{4.2}$$

$$\mathbf{V}_{\perp} = \mathbf{V} - \mathbf{V}_{\parallel} \tag{4.3}$$

$$T = \frac{2\ T_{\perp} + T_{\parallel}}{3} \tag{4.4}$$

$$p_{\text{plasma}} = N_p\ k_B\ T \tag{4.5}$$

$$p_{\text{mag}} = \frac{B^2}{2\ \mu_0} \tag{4.6}$$

$$\beta = \frac{p_{\text{plasma}}}{p_{\text{mag}}} \tag{4.7}$$

$$p_{\text{tot}} = p_{\text{plasma}} + p_{\text{mag}} \tag{4.8}$$

$$\mathbf{E} = -\mathbf{V}\times\mathbf{B} \tag{4.9}$$

$\mathbf{V}_{\parallel}$ is the plasma-velocity parallel to the magnetic field $\mathbf{B}$, while $\mathbf{V}_{\perp}$ is the velocity perpendicular to it.
T is the plasma-temperature calculated from the quantities $T_{\parallel}$ and $T_{\perp}$.
The *plasma* or *thermal pressure*, p_{plasma}, is given by the ideal gas equation.
The *magnetic pressure*, p_{mag}, is caused by an external magnetic field B and simply adds to the thermal pressure of a plasma, yielding the total pressure, p_{tot}. In equilibrium for an isotropic and quasineutral plasma the total pressure

is constant and the *plasma beta* is defined as the ratio of thermal and magnetic pressure (see Appendix).
Low β-values ($\beta \ll 1$) are found where the external magnetic field is strong compared to the thermal pressure. High β-values ($\beta \geqslant 1$) occur when the field is weak, for example in the neutral sheet. This parameter is very suitable to decide, whether to be inside the neutral sheet or not and will be an important criterion in this context.
The last parameter, calculated from velocity and magnetic field, is the electric field **E**. It is not necessary to calculate it, as it is measured by the **EFW**, *Electric Field and Wave*-experiment of the Cluster Mission, but for this purpose the accuracy achieved by the calculation was good enough. Also it could be used to compare it to the measurement.

Again everything was stored in a new structure with the following fields:

`FGM_t`	time of FGM-value
`FGM_xyz`	position of spacecraft
`B_xyz`	magnetic field; x,y,z-component
`B_tot`	total magnetic field
`CIS_t`	time of plasma parameters
`N_p`	particle density of protons
`V_pxyz`	ion-velocity in GSM-coordinates
`Vxyz_pperp`	ion-velocity perpendicular to magnetic field
`T`	temperature of plasma
`beta`	plasma beta
`E_xyz`	electric field 3-dimensional vector
`p_plasma`	plasma pressure
`p_total`	total pressure

and file name

```
CIS2004augustSC4
```

for the file of August 2004 of spacecraft 4.

Unfortunately the CIS-experiment on spacecraft Cluster 2 was damaged soon after launch, in an early state of the mission. As a consequence the plasma data is only available for the other 3 spacecraft.

4.1.4 Curlometer

The special feature of the Cluster Mission is a 4-point measurement in space. Difference measurements of the magnetic field can be used to derive a range of further parameters like gradient, current density vector, wave vectors or curvatures.
Depending on the scale-size of an observed or expected phenomenon L, compared to the spacecraft-separation R_{ij}, there are 3 different techniques:

Curlometer	$L > R_{ij}$
Wave Telescope	$L \approx R_{ij}$
Discontinuity Analyzer	$L < R_{ij}$

Magnetic reconnection is a small-scale phenomenon. To calculate the current density the Curlometer-method is used.
From Maxwell's equation, MHD-equation IV, the current density vector can be calculated from the curl of the magnetic field vector:

$$\text{IV.} \qquad \nabla \times \mathbf{B} = \mu_0 \mathbf{j} \tag{4.10}$$

$$\nabla \times \mathbf{B} = \begin{pmatrix} \frac{\partial B_z}{\partial y} - \frac{\partial B_y}{\partial z} \\ \frac{\partial B_x}{\partial z} - \frac{\partial B_z}{\partial x} \\ \frac{\partial B_y}{\partial x} - \frac{\partial B_x}{\partial y} \end{pmatrix} \tag{4.11}$$

According to [Khu96] the spatial gradients can be related to differences in the magnetic field measurements and the inter spacecraft distance in the following way.
First choose one spacecraft to be the mother spacecraft, let this be spacecraft one for example, which acts as a reference point for all difference calculations. The other spacecraft are so called daughter spacecraft.
We have 4 vector measurements, each at a vertex of the tetrahedron, $\mathbf{B}_i = (B_{xi}, B_{yi}, B_{zi})$ (for i=1,2,3,4).
A Taylor serious expansion about the center of mass 0 can relate spatial gradients to the measurements. The magnetic field at the point 0 is eliminated by subtracting out magnetic field components of spacecraft 1 from the magnetic field components of the other three spacecraft:

$$B_{x21} = \frac{\partial B_y}{\partial x} dx_{21} + \frac{\partial B_x}{\partial y} dy_{21} + \frac{\partial B_x}{\partial z} dz_{21} \tag{4.12}$$

$$B_{x31} = \frac{\partial B_y}{\partial x} dx_{31} + \frac{\partial B_x}{\partial y} dy_{31} + \frac{\partial B_x}{\partial z} dz_{31} \tag{4.13}$$

$$B_{x41} = \frac{\partial B_y}{\partial x} dx_{41} + \frac{\partial B_x}{\partial y} dy_{41} + \frac{\partial B_x}{\partial z} dz_{41} \tag{4.14}$$

B_{xi1}... difference between x-component mother spacecraft 1 and daughter spacecraft i
dx_{i1}... distance between spacecraft i and mother spacecraft 1

These equations relate the differences in x-component of the magnetic field and the spacecraft separations to the first order gradients of B_x.

$$\begin{pmatrix} B_{x21} \\ B_{x31} \\ B_{x41} \end{pmatrix} = \begin{pmatrix} dx_{21} & dy_{21} & dz_{21} \\ dx_{31} & dy_{31} & dz_{31} \\ dx_{41} & dy_{41} & dz_{41} \end{pmatrix} \begin{pmatrix} \frac{\partial B_x}{\partial x} \\ \frac{\partial B_x}{\partial y} \\ \frac{\partial B_x}{\partial z} \end{pmatrix} \tag{4.15}$$

By inverting the distance matrix we obtain

$$\begin{pmatrix} \frac{\partial B_x}{\partial x} \\ \frac{\partial B_x}{\partial y} \\ \frac{\partial B_x}{\partial z} \end{pmatrix} = \begin{pmatrix} a_{21} & a_{21} & a_{21} \\ a_{31} & a_{31} & a_{31} \\ a_{41} & a_{41} & a_{41} \end{pmatrix} \begin{pmatrix} B_{x21} \\ B_{x31} \\ B_{x41} \end{pmatrix} . \tag{4.16}$$

In the same way y- and z-component are treated and spatial gradients are gained. Now curl B can be calculated and the current density vector obtained. Additional we can calculate the divergence of B,

$$\nabla \cdot \mathbf{B} = \begin{pmatrix} \frac{\partial B_x}{\partial x} \\ \frac{\partial B_y}{\partial y} \\ \frac{\partial B_z}{\partial z} \end{pmatrix} . \tag{4.17}$$

It is a good error-estimator, due to the fact that the magnetic field should be divergenceless.

This procedure is executed in the function `rotdivB.m`.

```
[curl_xyz,Div]=rotdivB(FGMC,eveday,t_anf,t_end)
```

The function can be used to determine the rotation and divergence values, for either a single point in time or for a vector of time values, a time interval.
The input variable `FGMC` is a (1×4)-cell with the element's index corresponding to the spacecraft number, of which a structure of data is stored in. The structure fields need to contain the values of time, magnetic field and position, e.g. for spacecraft 2:

```
FGMC{2}.FGM_t
FGMC{2}.FGM_xyz
FGMC{2}.B_xyz
```

The fact that the 4 spacecraft measurements are not taken simultaneously necessitates synchronization. If there is only one input argument, `FGMC`, it must contain a single point in time only and no synchronization has to be made. For a data-vector of several time values further input arguments are needed: the day of month `eveday` and optional the starting time (`t_anf`) and ending time (`t_end`) of the desired interval. For data-vectors of times a nearest-neighbor search is performed. The maximal time-shift is 2 seconds, as data has a 4 second-resolution.

Due to the fact that information on all 4 spacecraft is needed at once to calculate $\mathbf{j}$ this function is only used when necessary and the parameter is not calculated in the data-structures of FGM or CIS. The unit is changed during execution from the input unit of position $[R_E]$ and the input unit of magnetic field, $\mathbf{B}$, [nT] to [pT/km], as the unit of rotation and divergence.

4.2 Event Search

Observations and detection of magnetic reconnection in the magnetotail using Cluster mission data has been discussed and evaluated in a couple of studies in the past. Several reconnection events have been published and are approved exemplary encounters of reconnection.
The successive search of reconnection signature in Cluster data and its statistical interpretation was the objective of this study. What are the best criteria to find reconnection events? Reconnection has well known effects, but is the detection of such enough to be sure about the encounter of a reconnection event and which are other processes causing similar signatures? These were some of the basic questions to deal with, which occurred before and during the data analysis.

The signature of an x-line reconnection event in the magnetotail is well known. At the x-line magnetic field lines are disconnected and reconnected to different partners. The magnetic field can be canceling but shows a reversal in z-component (along x-direction). The reconnecting field line earthward of the x-line points northward and the fieldline tailward of the neutral line is directed southward due to the magnetic topology of the lobes .

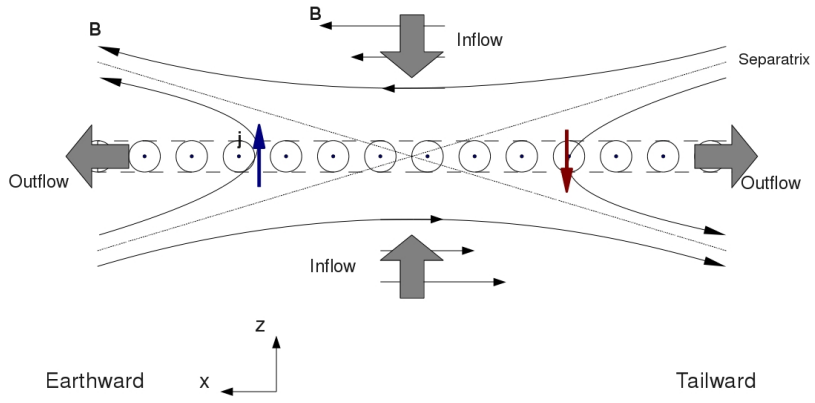

Figure 4.3: X-line

Newly reconnected field lines leave to both sides, tail and earthward. They are pulled away like gum strings, converting magnetic energy into acceleration of plasma. This is observable as plasma jets characterized by significant flow velocities in positive or negative x-direction. A spacecraft crossing the diffusion region or its vicinity encounters a reversal of significant flows correlated with the reversal in B_z.
Another criterion, we choose to determine in what part of the tail the spacecraft is, is the plasma beta. A high plasma beta of above 0.5 indicates that the

spacecraft crosses the plasma sheet or even the current sheet. This is the region we want high speed flows to be measured in case of reconnection. So finally we want high-speed flow reversal in x-direction with correlated B_z-reversal, all taking place in and close to the current sheet. The velocity-vector is split in 2 vectors: V-parallel $\mathbf{V}_{\parallel}$ and V-perpendicular $\mathbf{V}_{\perp}$.
$\mathbf{V}_{\parallel}$ is the velocity parallel to the magnetic field while $\mathbf{V}_{\perp}$ is accordingly perpendicular to the magnetic field. In the middle of the current sheet, there should be magnetic field only in z-direction (and y-direction) and flow mainly in x-direction, hence basically perpendicular flow velocity, as there are hardly any parallel components. Outside the current sheet the magnetic field adjusts systematically to lobe-topology and the z-component decreases. At the boundary of the plasma sheet flow in x-direction becomes more and more parallel to $\mathbf{B}$.

Concluding the reconnection-signature:

- B_z-reversal
- reversal of high speed flow $\mathbf{V}_{\perp x}$
- high plasma beta values $\beta > 0.5$

Observed reconnection events do not follow exactly the same pattern or appear in the same way. What method is the best to find all events, no matter how they occur in detail. Now one has several options.

First we performed a search to find significant negative B_z-values, $B_z < 10$, occurring in the outflow region of the x-line. Small negative values can be caused by oscillations or an effect of the coordinate system, while such values can not easily be explained that way. The Earth's magnetic dipole field is directed from south to north and positive B_z-values are expected. Significant negative values are therefore an evidence of B_z-reversal.
This resulted in only very few events. On the other hand small negative values can indicate reconnection as well and all these events are lost in this procedure.

4.2.1 $[\beta > 2\ , |\mathbf{V}_{\perp x}| > 300]$ -Events

The typical signature of an x-line event is $B_z V_x > 0$.
We started to find all plasma jets. An appropriate threshold is $|\mathbf{V}_{\perp x}| > 300$ km/s. Additional only times where plasma beta is $\beta > 2$ were retained.
The result was a list of all points in time, for which significant flow and a relatively high plasma beta are fulfilled simultaneously. Like significant negative B_z-values are an evidence of B_z-reversal, flow events are an evidence of acceleration, only the acceleration mechanism is not instantly apparent.
This collection of data is split into events. An event is a sequence of times that meet the criteria and consecutive times are within 30 minutes. Thus one event is separated from the next by at least 30 minutes. Only exception is a change of day. Later on we will refer to an event only by the time it starts and ends. Also the event is not assigned to a special spacecraft, but it is noted which spacecraft detect the same event or rather a coinciding event, at about that time.

The search is performed in the program `eventsuche_vx.m`. Concluding the criteria:

- $|\mathbf{V}_{\perp x}| > 300$ km/s
- $\beta > 2$
- time separating distinct events: > 30 min

We apply this search to data available for the following years:

2001, 2002, 2003, 2004, 2005, 2006, 2007,

during the tailseason, from July to October, per month. Results are stored in a structure, for each month and one spacecraft with the filename:

`Vperp_x_EVENTS`$<$ *year* $><$ *month* $><$ `Nr_SC` $>$

$<$ *year* $>$ is a string of the number of year, $<$ *month* $>$ is either juli, august, september or oktober corresponding to month 7 to 10, respectively. $<$ `Nr_SC` $>$ is of course the number of spacecraft, 1, 3 or 4. Cluster 2 offers no plasma-data for the search.
The $1\times <$ *daysofmonth* $>$-structure consists of several fields:

`event_anzahl`	total number of events found for one day of month and spacecraft
`day`	day of month only if events are found that day
`event`	$1 \times n$-structure of n events

$<$ *daysofmonth* $>$ is 30 or 31 depending on the month and its number of days. The field `event_anzahl` has an index for each day which contains the number of events found that day. If no events are found that day, the field is empty. Just like the field `day`, which only contains the number of day, if any events have been found. The `event`-field is also a structure with fields:

```
event_ind
Vperp_xmax
Vperp_xmaxind
t_min
eventanfang
eventende
B_xyz_minind
B_tot_minind
N_p_minind
T_minind
beta_minind
E_xyz_minind
V_xyz_minind
Vperp_xyz_minind
FGM_xyz_minind
```

Each event of the day is one index of the structure, for 2 events of day 28 for example it is a 1×2-structure. The value in field `event_index` is a vector of indices. These indices correspond to the indices of the values in the CIS-data-structure, of the specific day that were filtered out.
Supplementary some main-values of the event were saved in the structure: the maximum value of $|\mathbf{V}_{\perp x}|$ during the event `Vperp_xmax` and its index `Vperp_xmaxind`, the time belonging to that value in `t_min`, the beginning `eventanfang` and the ending-time `eventende` of the event, and other plasma and magnetic field values of the time of maximum of $|\mathbf{V}_{\perp x}|$, denoted by the parameter's name with an `ind` attached to it.

The next step was to compare the encountered events of different spacecraft to each other. For this purpose all events, no matter which spacecraft they were detected by, are listed. Events of different spacecraft that are within ten minutes, based on the time of maximum flow-velocity, are saved as a single event, only once. The program named `eventlist_month_vx_perp` not only extracts or concludes the events and aborts copies, but also saves the list as a matrix of start and ending time, time of maximum absolute flow and its corresponding plasma and magnetic field values in the file

`Vperp_x_EVENTmatrix`$<$ *year* $><$ *month* $>$`all`.

One column in the list reveals, what spacecraft the event was detected by and the measured values in the list belong to. An additional column notes, which spacecraft also detected events within 10 minutes of the maximum value.
The list is the basis to plot the events and have a look, whether our criteria, to filter the required events, succeeded.

4.3 Eventplot

Detection of reconnection is not an easy task. Since reconnection is a complex phenomenon and Cluster can only utilize a limited observation region, various detection-patterns, caused by reconnection, are possible. There is no typical pattern one can expect to find in data. Thus a simple pattern recognition program wouldn't work and the resulting events of our search were inspected visually.
A plot program `eventplot_month_vx_perp.m` was developed to plot the events of the list of each month separately. We decided that the average time of a reconnection event is about an hour and took that value as the plot range for all parameters. Taking the time of maximum flow-velocity in x-direction as the center and plotting 30 minutes before and after that time was chosen to yield the 1 hour time span. Of course some events can not be fully covered by a 1 hour plot, but for a first selection of reconnection events it is long enough and more convenient than longer periods of time, especially because of a higher resolution of time in the plot.
Each plot has a high number of panels. Almost all parameters of the CIS-dataset including the magnetic field were plotted one below the other.

One plot consists of 13 panels with 14 parameters displayed. From top to

panel	parameter	unit
1	B_x	[nT]
2	B_y	[nT]
3	B_z	[nT]
4	B_{tot}	[nT]
5	$(\nabla \times B)_y$ and $\nabla \cdot B$ (pink)	[pT/km]
6	E_y	[mV/m]
7	V_x	[km/s]
8	$V_{\perp x}$	[km/s]
9	V_y	[km/s]
10	V_z	[km/s]
11	N	[cm^{-3}]
12	T	[MK]
13	β	

Table 4.3: List of panels of the plot created in the eventplot-program

bottom these are shown in the table 4.3.

What are the main parameters to look at?
First of all we have a look at B_z and $V_{\perp x}$. Whether they have a reversal and if it is correlated or not.
Then we want to know, if we are in the current sheet. The parameters β and j_y, respectively curl B, can reveal that. The plasma beta should be high as in our criterion and if sufficient currents flow, as expected in the current sheet mainly in y-direction, this parameter should also be high. But what does high mean in that context? That's why we're plotting the divergence of B in pink color in the same panel, number 5. The result of rotation B is only reliable if the divergence is small, using the Curlometer method. Multiplying curl B (in pT/km) by $\frac{10}{4\pi}$, yields the current density in nA/m^2. The main current sheet has a typical thickness of 1-2 R_E and the current density is in the order of some nA/m^2 [BT96]. For thin current sheets, for example near the x-line, the current density can be even higher.
Another indicator, how far the spacecraft is from the neutral sheet, is B_x. In the neutral sheet the entire x-component of the magnetic field is expected to vanish. When passing the neutral sheet, B_x should decrease and $|B_z|$ should increase. Sometimes this is not the case for B_x. One reason may be that the coordinate system is tilted with respect to the actual alignment of the tail at that time. It does not fit the tail system like in theory, due to its variation with the solar wind-influence.
If the current sheet is thin, B_x may be high even if the measurement is taken in its vicinity. A spacecraft travelling parallel to the current sheet may even detect increasing B_x when passing a reconnection region or x-line.
Typical values of the particle density are found in table 4.4. If the particle density is low, the spacecraft is in the lobes. Though if the particle density is high the spacecraft is not necessarily in the plasma sheet or current sheet. High values are also expected in the magnetosheath. Nevertheless N has to be high while passing the plasma sheet.
Temperature and plasma beta are in logarithmic scale.

Region	N [cm^{-3}]	B [nT]	β
Magnetosheath	8	15	2.5
Tail lobe	0.01	20	$3\ 10^{-3}$
PSBL	0.1	20	10^{-1}
CPS	0.3	10	6

Table 4.4: Typical values of particle density N, magnetic field and plasma beta, expected to be found in different regions in the magnetotail. PSBL is the plasmasheet boundary layer in between the plasma sheet and the tail lobes and CPS is the central plasma sheet. [RK95]

A B_x-reversal indicates a current sheet crossing. Positive B_x is found in the north-lobe and negative in the south-lobe, where the magnetic field is directed away from the Earth.
The parameter B_y is about zero in mid september, when the spacecraft has a noon midnight orbit and is therefore in the middle of the tail in y-direction. In the region away from midnight a B_y-component appears due to a slight tilt of the magnetic field toward the radial direction from the Earth. B_y can also be an indicator of a Hall-magnetic field.
If a negative B_y is found the field is pointing dawnward in y-direction. For a positive $B_y > 0$ it points duskward.
Last but not least a missing reversal in B_z can also be caused by an offset-error.

In a first sort out procedure all events were visually inspected and those, which had none of the required characteristics were discarded. The remaining events were classified as either *pink* or *yellow events*.

Pink events are high speed flow-events that don't show reversal in B_z but sometimes with disturbance in B_z. Therefore they are not typical reconnection events, but plasma has been accelerated by some cause maybe related to reconnection.

Yellow events are those, which include both, B_z-reversal and flow-reversal. In some cases the B_z reversal was very small and not very clear. All these interesting events were inspected in detail using additional plots available at Cluster Active Archive (CAA).

Sometimes B_z-reversal is found together with the reversal of high speed flow and is nevertheless no x-line event. An o-line event has a similar signature like an x-line event. The o-line is a neutral line in the center of a *plasmoid*, the closed loop fieldline formed structure occurring during substorms.

There are various phenomena with similar signatures, but different physical origin. One of these is the so called flux rope. A flux rope moving past the spacecraft causes a bipolar B_z-variation. A closed-loop plasmoid is a specific type of a flux rope. Its size depends on the formation process and the location it is detected. They are observed in a broad range of sizes.
A plasmoid forming in between the near-Earth x-line and the distant x-line is often driven tailward at high speed.

These large plasmoids can be measured in a wide region around the central plane. Inside the plasmoid the field lines form closed loops and the magnetic field strength is small and zero in the middle. The magnetic field outside is compressed by the plasmoid and the field strength increases. Due to its form Cluster measurements can show a reversal in B_z, even if the spacecraft are far from the current sheet, together with a plasma flow, carried by the plasmoid. In such a case it is helpful to look at the current density j_y. If the current density is small, the spacecraft is not in the current sheet, hence it cannot be a reconnection event, or x-line.
Another example of flux ropes is produced by multiple x-line reconnection. This leads to the formation of islands, multiple magnetic loops. Often they increase in size as they move downtail. Small flux ropes are associated with high speed flow. An earthward flux rope is called busty-bulk-flow-type flux rope, while a tailward travelling one is called plasmoid-type. In all places in a flux rope the current is field aligned, $\mathbf{j} \times \mathbf{B} = 0$.
If we are in the current sheet discovering an o-line phenomenon, B_z- and the flow-reversal are anticorrelated.
Another possible encountered effect, causing B_z-reversal, may be localized reconnection or field aligned currents.
In a localized reconnection process a non-zero guiding field (B_y) produces a reversal, when it gets twisted in the middle of the current sheet by a plasma jet. The resulting signature is a B_z-reversal together with increasing flow speed.
A plasma bubble is a structure with field aligned currents, transporting flow beyond the current sheet. Due to its structure positive and negative B_z-orientation is produced. The alignment of currents in the bubble is very similar to the substorm current wedge. The current wedge forms together with the near-Earth neutral line. Tail-like field lines collapse to form a dipolar configuration, associated with the field dipolarization caused by x-line reconnection.
We tried to avoid taking these similar signatures into account in our x-line filtering procedure. O-line events are classified as *pink*.

There are also high speed flow events caused by a solar wind detection. Indicated by a high B_y value and a high particle density N, or a change in N, the spacecraft crosses the outer boundary of the magnetosphere, the magnetopause, and detects solar wind particles and high speed flow.
In 2006 the orbit was changed and the Cluster formation crossed the current sheet at a smaller distance of around 12 R_E.

To check the *yellow events* again and more in detail to decide if they are likely to be really x-line encounters we used the CAA graphical product. On the website `http://caa.estec.esa.int/caa_graphics/graphics.xml`, after login it is possible to plot up to seven panels of different parameters on demand. This was done for all *yellow events*, using the pregenerated one-hour plot option, showing the following panels of table 4.3 from top to bottom.

The time range was again chosen to be half an hour before and after the maximum of flow. Sometimes, when data gaps of Cluster 3 appeared, the upper two panels were changed from Cluster 3 values to values of Cluster 1, keeping the same parameters and instruments. In other cases additional plots of longer

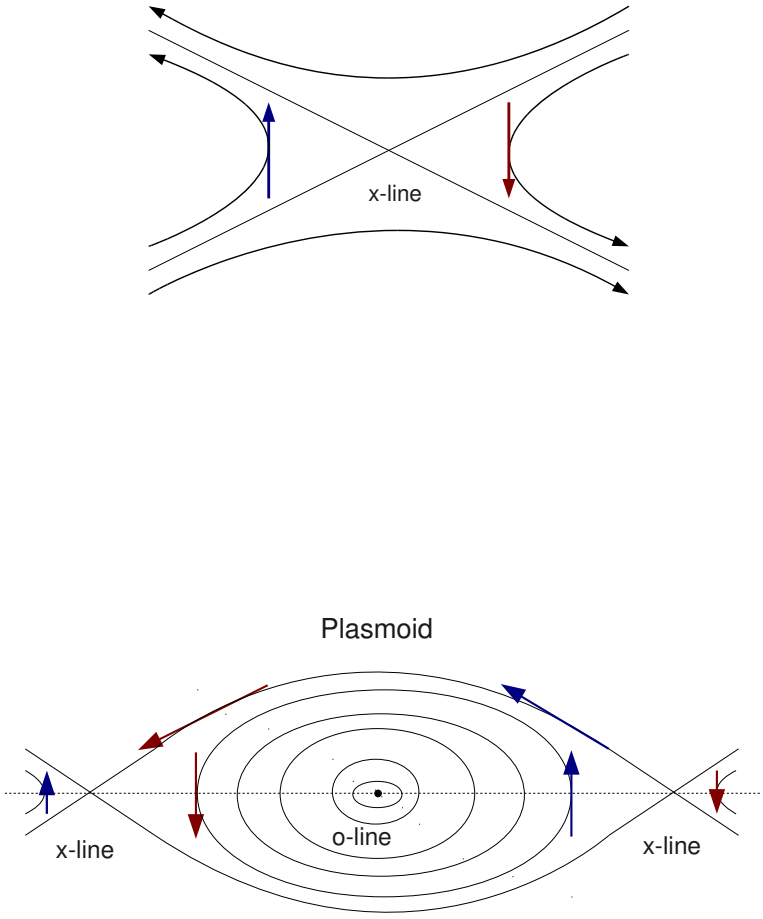

Figure 4.4: Simple 2-dimensional view in xz-plane. X- and O-lines are the dots in the center, each building a line perpendicular to the plane of the figure in y-direction. The plasmoids inner structure may be much more complicated. The red and blue colored arrows are emphasized to show the magnetic z-component reversal, which is found in both x- and o-line encounter. It is also apparent that in the central plane the z-component around the o-line is oppositely directed to the one around the x-line. The plasmoid, also carrying plasma-flow as it moves, can cause a z-component reversal of the magnetic field even away from the central plane (dotted line).

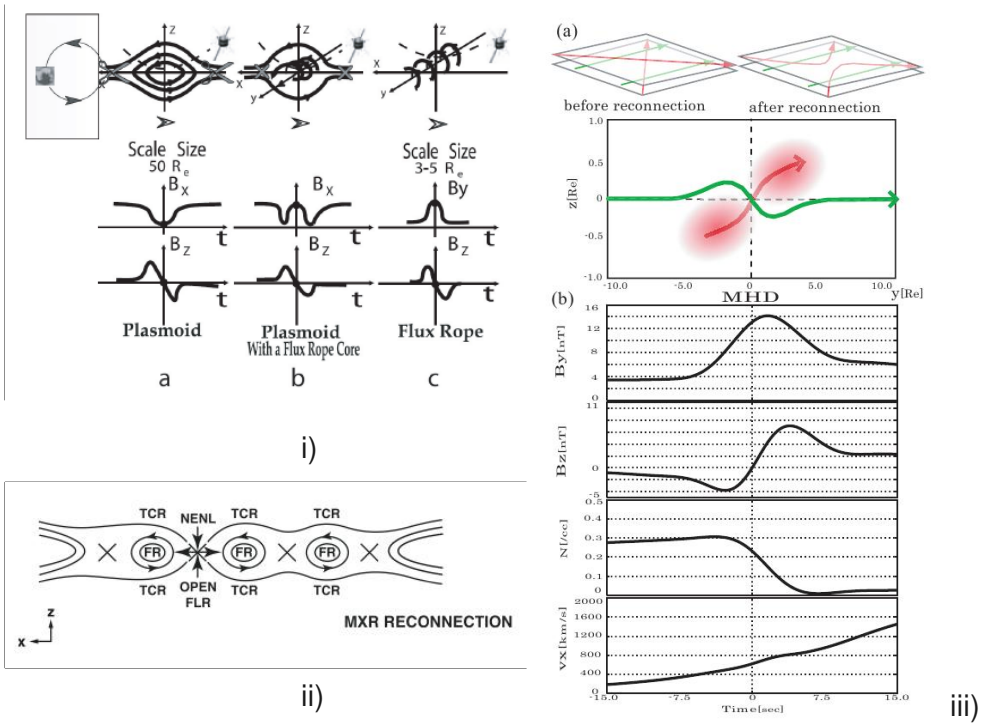

Figure 4.5: In i) different forms of flux ropes together with their signature are shown. ii) is an outline of multiple x-line reconnection MRX. In iii) the localized reconnection process is illustrated. Red lines are reconnected and green lines are current sheet field lines.[SNR+08]

time-periods were created, if the event-time of interest seemed to extend longer than one hour.
The upper 2 panels show the magnetic field component of interest B_z and the velocity V_x. The next 4 panels contain PEACE plots of the electron energy spectrogram of all 4 Cluster measurements. These are used to check, whether electrons have been accelerated or not. The last panel displays the energetic electron spectrogram of the RAPID measurement on Cluster 3.

Together with the original plots, the newly created plots were used in a second sort out procedure. It was distinguished between 3 different groups: again a group of *yellow events*, standing for the best events found, a group of *orange events* and *white events*.
An event was classified as an ***orange event***, if the flow and B_z-reversal were uncorrelated.
White events were those with flow reversal, but only an offset-B_z-reversal, meaning there was no real B_z-reversal, but a B_z-signature similar to reconnection. Considering an offset-error such an event would be a correlated reversal and therefor an x-line event.

	shortcut	instrument
B_z	C3 FGM SPIN	Cluster 3 FGM-data in GSE-coordinate
V_x	C3 CIS PP	Cluster 3 CIS-data in GSE
E1	C1 PEA	electron Energy spectrogram (omnidirectional) of PEACE on Cluster 1
E2	C2 PEA	electron energy spectrogram (omnidirectional) of PEACE on Cluster 2
E3	C3 PEA	electron energy spectrogram (omnidirectional) of PEACE on Cluster 3
E4	C4 PEA	electron energy spectrogram (omnidirectional) of PEACE on Cluster 4
Ee	C3 RAP	energetic electron spectrogram (omnidir.) of RAPID on Cluster 3

Table 4.5: Plot-parameter used in CAA graphical plot tool

And ***yellow events***, looking like perfect x-line like events with correlated reversal in flow and B_z.
Some of the former yellow events were even downgraded as ***pink events*** because it was discovered that one of the reversals was not clear enough.

Finally 50 events were retained as typical x-line like, yellow events. Those were used for further investigations.

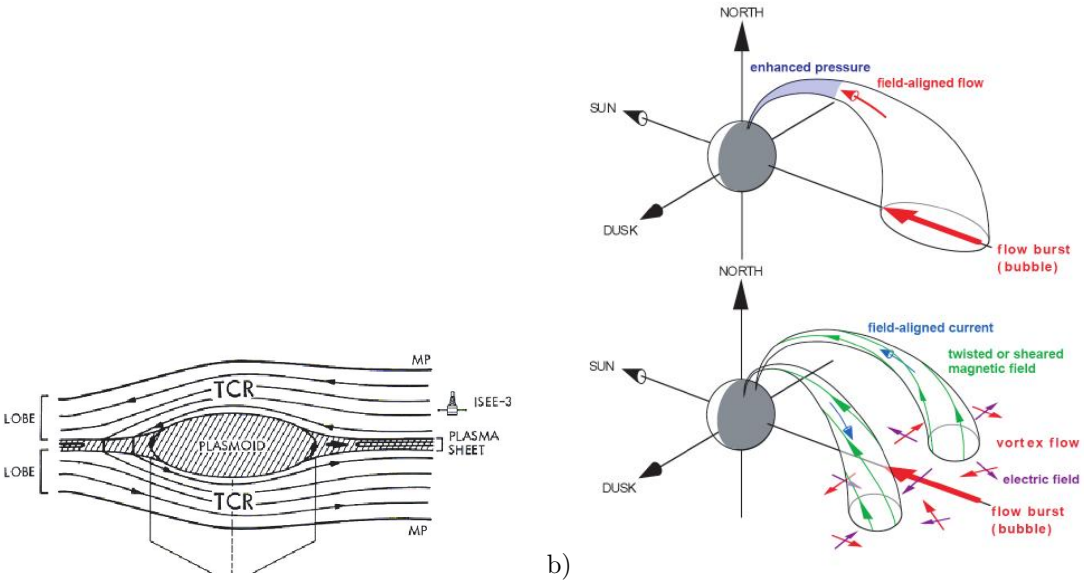

Figure 4.6: Possible causes of B_z-reversal are plasmoids like the travelling compression region (TCR) in a), or a plasma bubble in b). Both taken from [SNR+08]

4.4 Best Events

For the best x-line like events, the group of yellow events, one more specification had to be made.
The search algorithm filtered out all data meeting the flow-criterion of $|\mathbf{V}_{\perp x}| >$ 300 km/s with $\beta > 2$ and merged them to different events, as described before. Only an actual event doesn't start with 300 km/s-flow, but before. The same is true for the event-ending, which takes place a little after the high speed flow. Our events started with the first data point of the criterion and ended with the last of the specific event.
But what is an appropriate procedure for automation to find the real beginning and end of an event? Several procedures were considered, examined and compared to each other for a limited number of events.

The fact that we now already had the approximate time of an event simplified thinking about possible criteria. The plasma beta was not needed anymore as the criterion for the current sheet. Due to the fact that in the current sheet zero flow-velocity is hardly found at any time, except for flow-reversal of course, the quiet time velocity was estimated as about 100 km/s, or in other words the onset time of an event.

Criterion: $|\mathbf{V}_{\perp x}| >$100 km/s

The problem with this criterion was that the length of an interval and the duration of the event became very long, much too long for a real x-line event, because the criterion was met very often. So we decided to choose a value in between the quiet-time 100 km/s-value and our high speed threshold value of 300 km/s.

Criterion: $|\mathbf{V}_{\perp x}| >$200 km/s

The results in this case were better, but unfortunately in many cases totally inappropriate and not corresponding to the real onset and end time of the event. As one last option we simply tried out the 300 km/s threshold, even though this would not lead to the expected time. The difference to the original event search criterion was only the absent plasma beta criterion.

Criterion: $|\mathbf{V}_{\perp x}| >$300 km/s

Compared to the original criterion, all of the considered methods could not provide significant improvement of the estimated time. So we took the list from the original search criterion and compared it to the visual estimation of start and end time. Some events were left unchanged in their times, but many were changed to better visual estimations. This was of course only possible due to the small number of final yellow events of 50.

In the following we will have a look at some of the events, representative for the results in the list of yellow events, before the discussion of statistical results.

4.5 Examples of Yellow Events

Here are some examples of the event-plots, classified as yellow or x-line like events. In each panel there are multiple lines. The black line is the parameter measured by Cluster 1, red is Cluster 2, the green line is data from Cluster 3 and blue corresponds to Cluster 4, according to the general convention.
The vertical line marks the time of maximum flow in our criterion, together with $\beta > 2$.
The pink stars in the last panel indicate the automatically determined starting and ending time of the event.
In panel number 6 (from top) the pink line is the divergence of B, $\nabla \cdot \mathbf{B}$, calculated with the Curlometer method and is an estimator of the reliability of the simultaneously calculated rotation of B, $\nabla \times \mathbf{B}$. The closer the divergence approaches zero, the more we can trust the value of the rotation, which is the other line in this panel, in color of the spacecraft that encountered the event.
Data gaps were not interpolated and are visible as interruption of the lines. For cumulative gaps the line seems to be dotted sometimes.

4.5.1 Event on 14$^{\text{th}}$ August 2002

During the tail season of 2002 the Cluster satellites were forming a regular tetrahedron, 4000 km separated from each other. In August the orbit is not yet in the midnight meridian, but on the dusk side.
The event starts with the upcoming tailward flow at 3:58 UT, accelerated to a perpendicular velocity in x-component of more than 600 km/s. This flow is correlated with a negative B_z-value of up to -9 nT (Cluster 3). At 4:12 UT an earthward flow is enhanced with a maximum velocity of 1445 km/s at 4:14 UT. Again the flow is correlated with a positive B_z. Due to many data-gaps the flow was mainly detected by Cluster 4. In the uppermost panel it becomes clear that all spacecraft enter at the beginning of the plot from the north lobe and change the lobes at the beginning of the interval of interest. Especially Cluster 4 has several neutral sheet crossings during this interval, which lasts until 4:18 UT. So the satellites are temporarily in different hemispheres. Together with the fact that intense current is present, we are for sure in the thin current sheet and a reconnection event has been detected.
Also the interval start- and end-time detection, denoted by the pink stars in the last panel, was satisfying and corresponds well to the actual interval duration. During the entire interval there is another flow reversal at about 4:12 UT. The reversal is also visible in B_z. This shows that the events are not as simple as expected in theory.

4.5.2 Event on 28$^{\text{th}}$ August 2002

An even clearer example of a reconnection event is the one on August 28 2002 starting at 9:53 with the encounter of a strong earthward flow of -645 km/s ($\mathbf{V}_{\perp x}$) detected by spacecraft 4. Cluster 1 and 3 also detect a tailward flow, but mainly in the full $\mathbf{V}_x$-component and only a smaller value in the component perpendicular to the magnetic field. The flow is again well correlated with a

negative B_z-value of about -10 nT, seen by all satellites. The B_z progression is very clear at that time.
The flow reversal takes place at 10:06 UT first detected by Cluster 4 and time-shifted by Cluster 1 and then 3. This correlates very well with the sequence of the neutral-sheet crossing (panel 1). Cluster 4 changes the hemisphere before Cluster 2 followed by Cluster 1. Cluster 3 crosses the neutral sheet at last. The positive flow is accompanied by an instant change of B_z to a positive value, but not strong at first. At 10:15 UT B_z shows a quite complicated structure.There are several reversals in B_z, more than in V_x.
The flow continues but not steadily and during that period B_z is at maximum 12 nT. For a good event, we hope to find maxima of B_z and V_x occurring at the same time. This is not the case here. One reason for this may be lobe-reconnection, or simply a complicated configuration.
The event ends at around 10:29 UT. At maximum flow times intense currents are obtained. The particle density N shows a decrease during both, tailward and earthward flow, associated with the character of a plasma jet being a tenuous flow.

4.5.3 Event on 13$^{\text{th}}$ September 2002

In mid September the orbit is close to the noon midnight plane. The event starts at 18:08 UT with a tailward flow. Its maximum speed is detected by spacecraft 4 with a velocity of 1244 km/s (18:10 UT). The correlated negative B_z-value is -10 nT at most (Cluster 3). About 10 minutes later significant earthward flow starts, with a lower maximum speed of 780 km/s, again detected by Cluster 3. The z-component of the magnetic field changes to a positive value, in analogy to the theory, with a maximum of about 8 nT. The fast flow activity decreases shortly, for about a minute, during a period of reversal of B_z, and restarts when the magnetic field component is positive again. Here B_z is more complicated than usually. This is typical for an o-line or plasmoid signature.
The B_x-panel reveals the lobe changes, especially for Cluster 3 several times and the very simultaneous fast flow detections during the neutral sheet crossing. The current is also significant and reliable, due to the small divergence (pink), during the entire plot period. The particle density becomes small during flow activity, showing the tenuous state of plasma.
At the time of the tailward flow Cluster 3 is found in the south lobe, while all other spacecraft are mainly in the north lobe. For these spacecraft a negative B_y-value is found, hence they see a dawnward directed y-component, while Cluster 3 sees a dusk-directed positive B_y. It seems that the formation probes the close vicinity of the diffusion region, as the separatrix is occasionally in between Cluster 3 and the others.
In this case the automatic detection of the start and ending time of the interval yielded a very good result, apparent in the pink stars in the last panel, which stand for the interval-limits.

The near-Earth neutral line (NENL) is often found in between 20 and 30 R_E down tail. Due to the orbit, the Cluster satellites observe many earthward flows. When we find the reconnection signature, we often see tailward flow first, followed by earthward flow. This can be associated with an x-line propagating

downtail, or equivalent Cluster moving earthward relative, to the x-line.

In all examples it becomes clear that plasma data of Cluster 3 is noisier than other spacecraft data. In the z-component of the velocity and in particle density it additionally has a relatively high offset. In order to minimize its influence, we mainly concentrate on Cluster 1 and 4 in the following statistical evaluation.

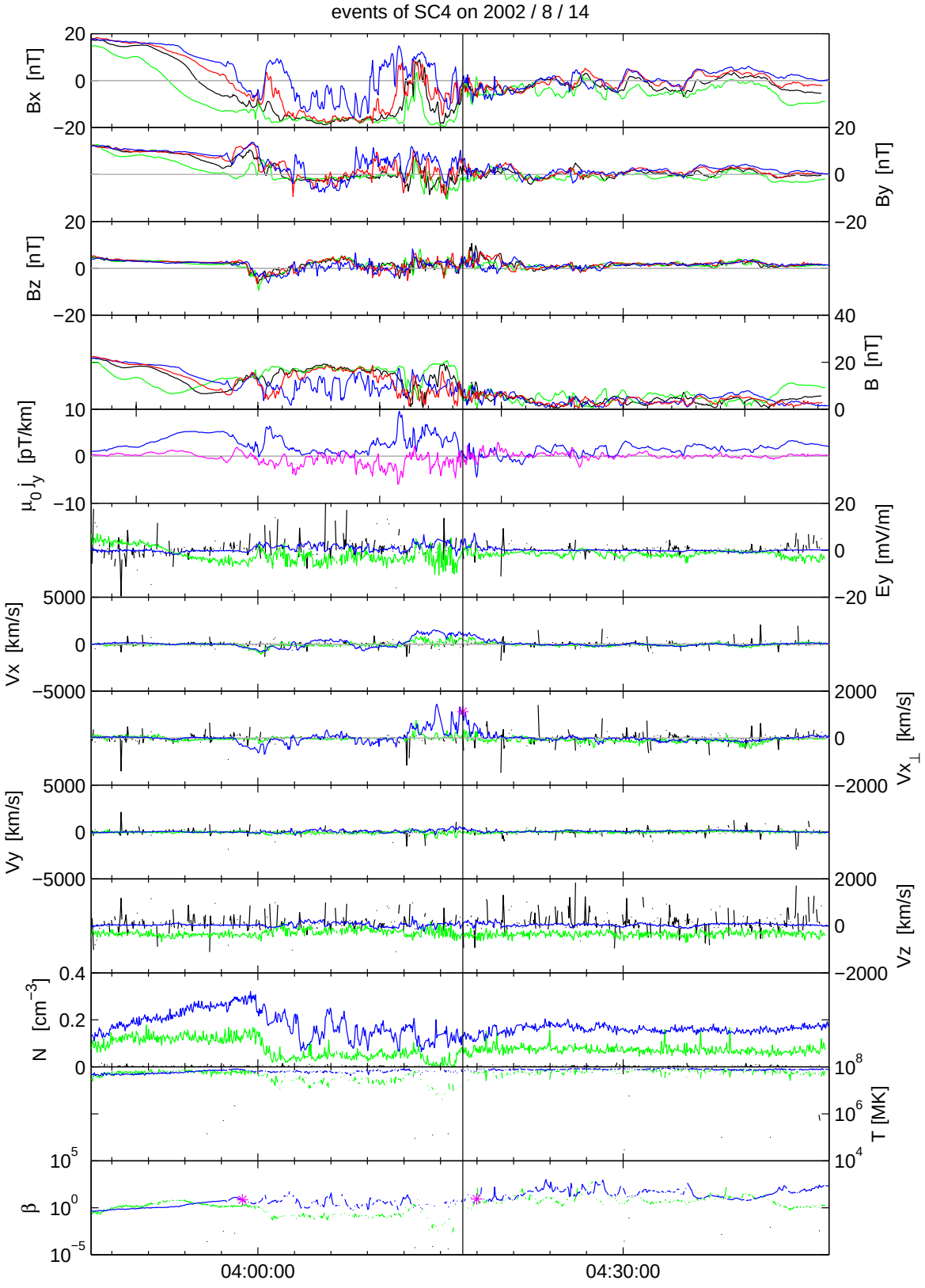
events of SC4 on 2002 / 8 / 14
Bx [nT]
By [nT]
Bz [nT]
B [nT]
μ0 jy [pT/km]
Ey [mV/m]
Vx [km/s]
Vx⊥ [km/s]
Vy [km/s]
Vz [km/s]
N [cm−3]
T [MK]
β
04:00:00
04:30:00

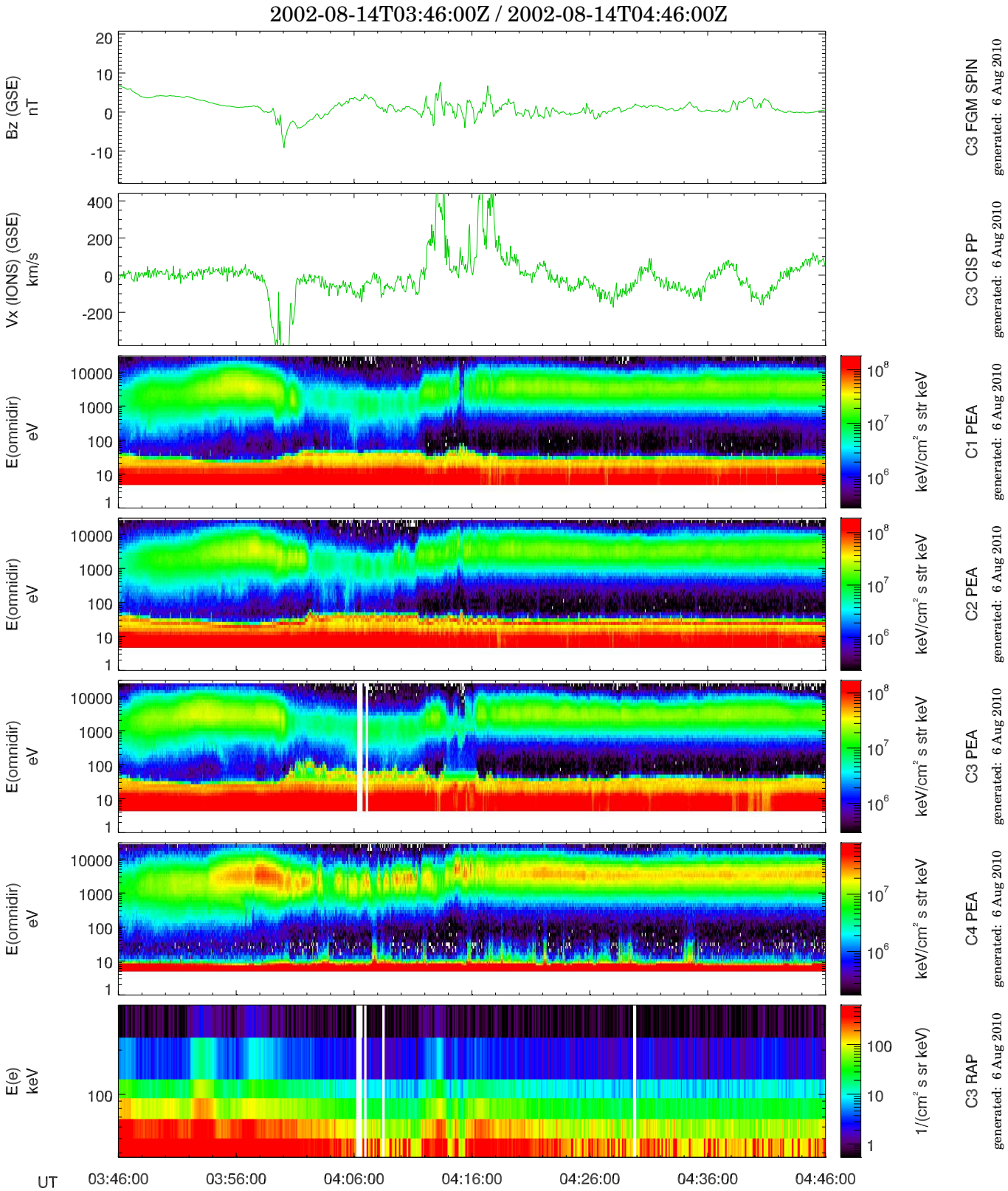
2002-08-14T03:46:00Z / 2002-08-14T04:46:00Z
Bz (GSE) nT
Vx (IONS) (GSE) km/s
E(omnidir) eV
E(omnidir) eV
E(omnidir) eV
E(omnidir) eV
E(e) keV
keV/cm² s str keV
keV/cm² s str keV
keV/cm² s str keV
keV/cm² s str keV
1/(cm² s sr keV)
C3 FGM SPIN
C3 CIS PP
C1 PEA
C2 PEA
C3 PEA
C4 PEA
C3 RAP
generated: 6 Aug 2010
UT
03:46:00
03:56:00
04:06:00
04:16:00
04:26:00
04:36:00
04:46:00

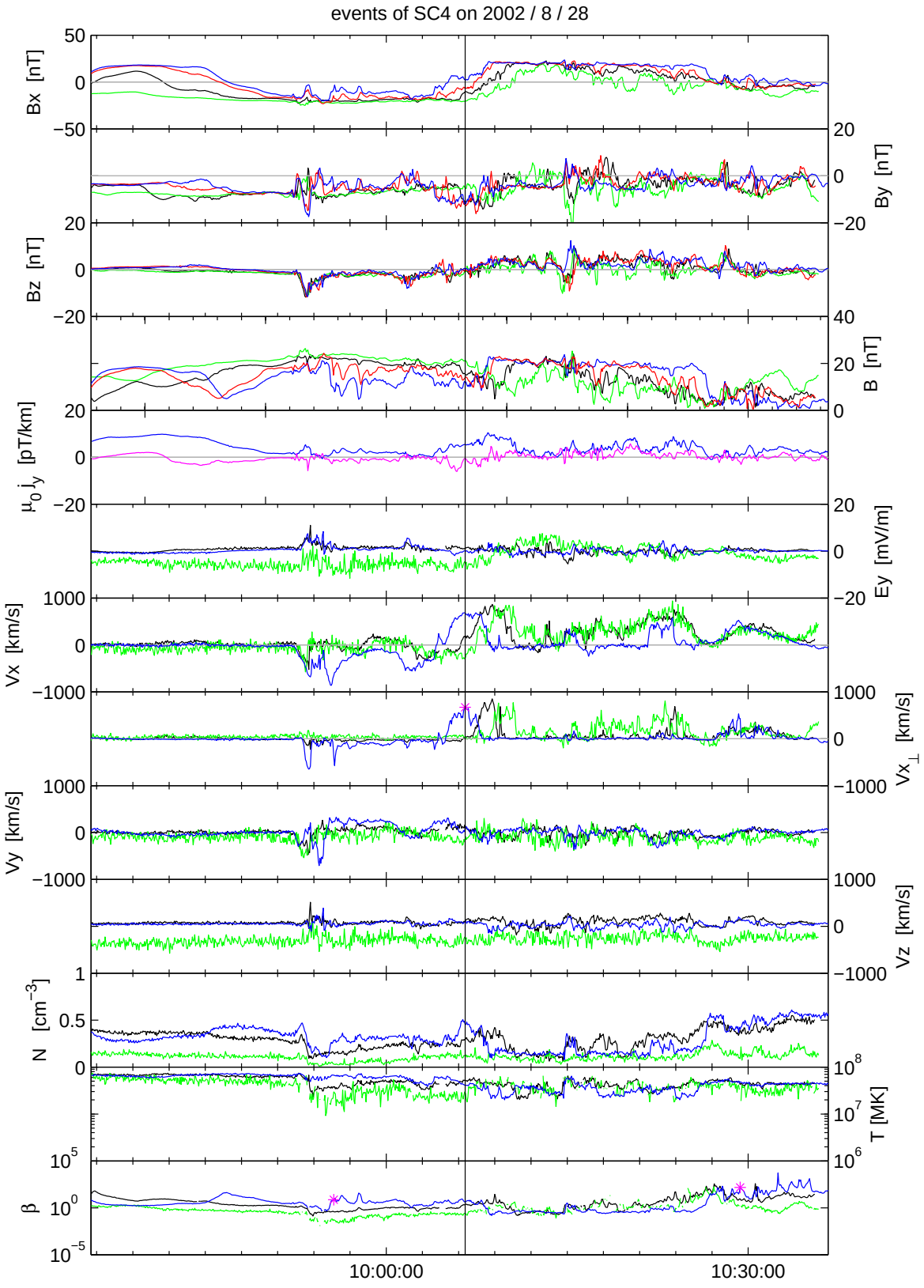
events of SC4 on 2002 / 8 / 28
Bx [nT]
By [nT]
Bz [nT]
B [nT]
μ0 jy [pT/km]
Ey [mV/m]
Vx [km/s]
Vx⊥ [km/s]
Vy [km/s]
Vz [km/s]
N [cm−3]
T [MK]
β
10:00:00
10:30:00

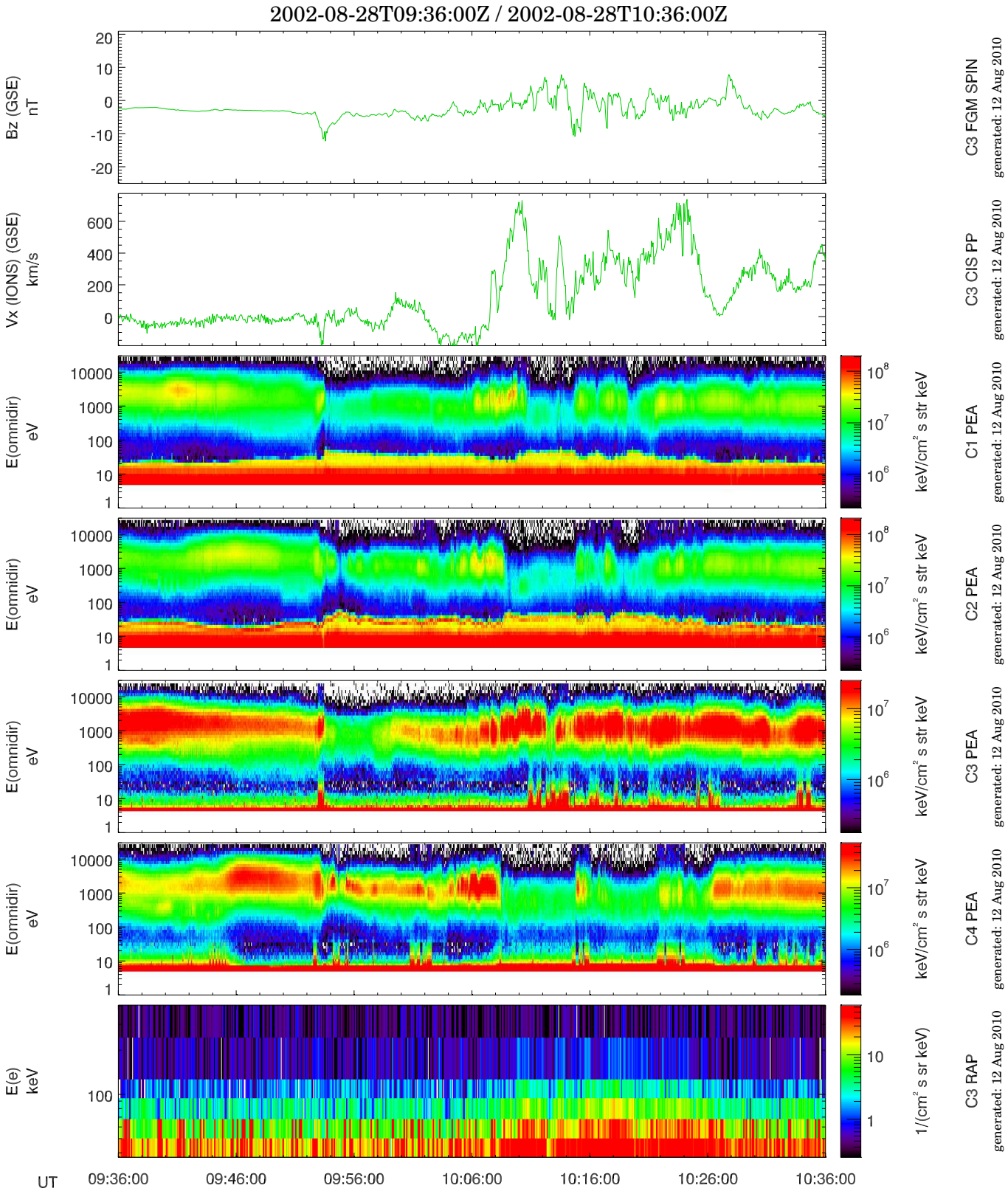
2002-08-28T09:36:00Z / 2002-08-28T10:36:00Z
Bz (GSE) nT
Vx (IONS) (GSE) km/s
E(omnidir) eV
E(e) keV
keV/cm² s str keV
1/(cm² s sr keV)
C3 FGM SPIN
C3 CIS PP
C1 PEA
C2 PEA
C3 PEA
C4 PEA
C3 RAP
generated: 12 Aug 2010
UT
09:36:00
09:46:00
09:56:00
10:06:00
10:16:00
10:26:00
10:36:00

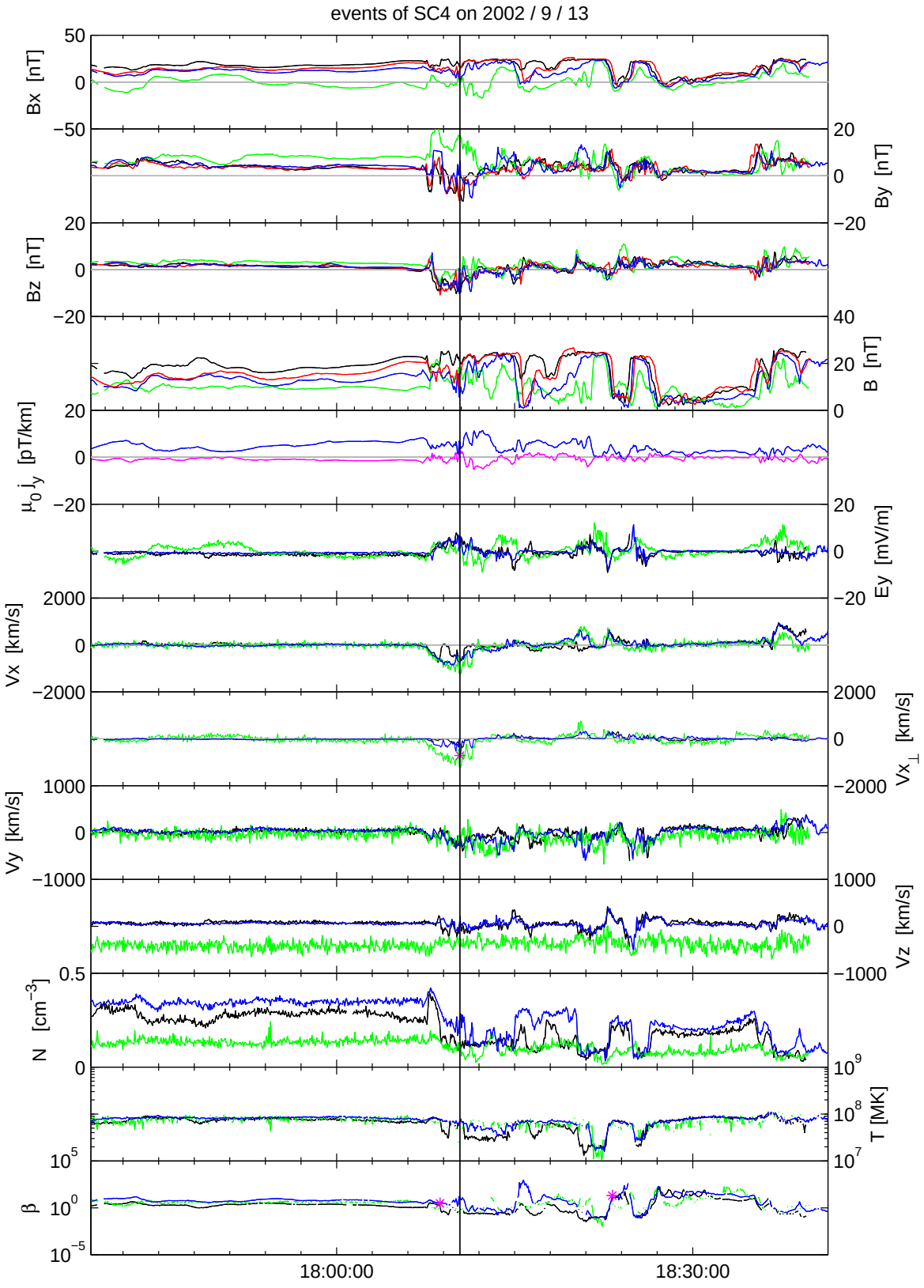
events of SC4 on 2002 / 9 / 13
Bx [nT]
By [nT]
Bz [nT]
B [nT]
μ0 jy [pT/km]
Ey [mV/m]
Vx [km/s]
Vx⊥ [km/s]
Vy [km/s]
Vz [km/s]
N [cm−3]
T [MK]
β
18:00:00
18:30:00

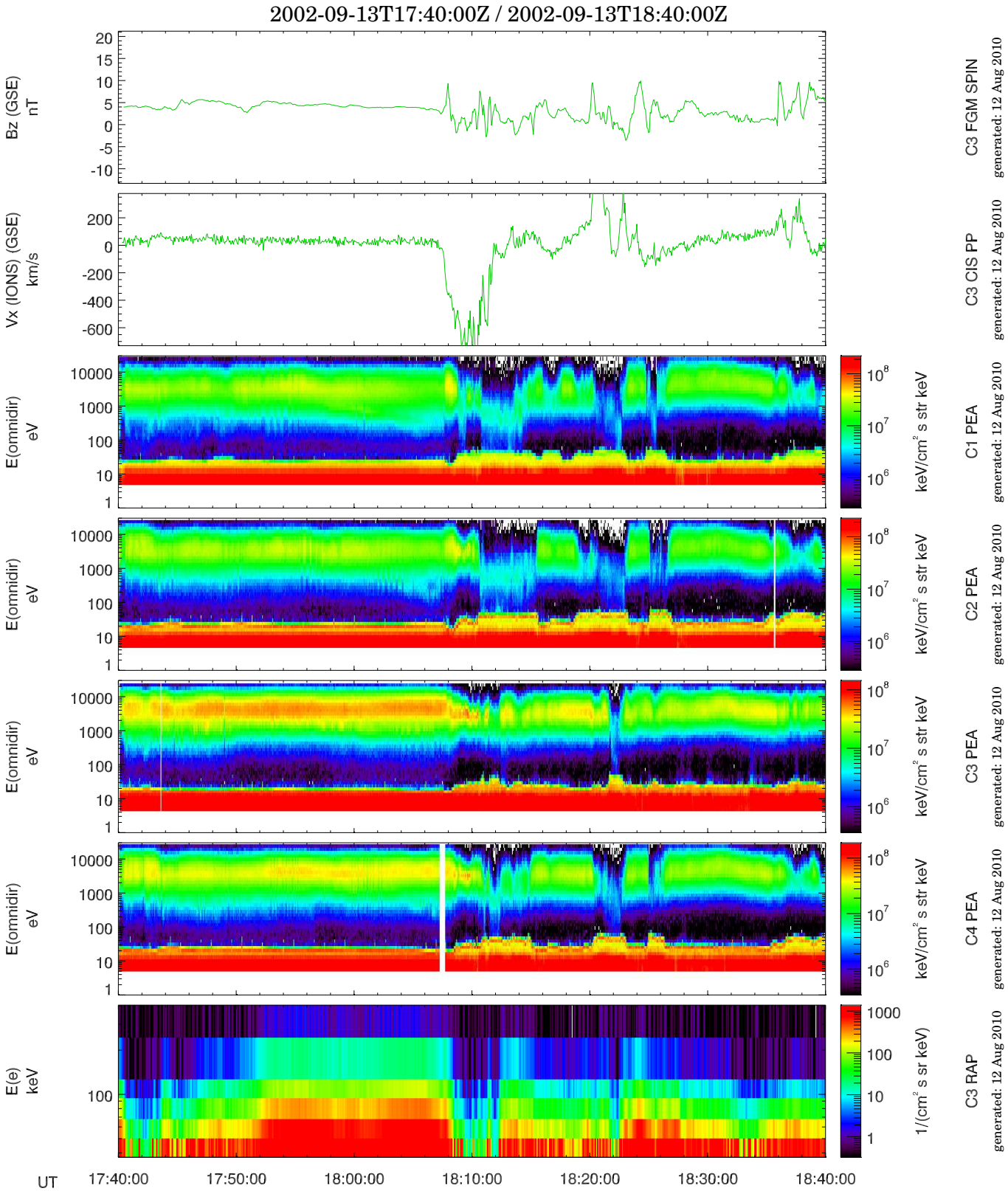
2002-09-13T17:40:00Z / 2002-09-13T18:40:00Z
Bz (GSE) nT
Vx (IONS) (GSE) km/s
E(omnidir) eV
E(e) keV
keV/cm² s str keV
1/(cm² s sr keV)
C3 FGM SPIN
C3 CIS PP
C1 PEA
C2 PEA
C3 PEA
C4 PEA
C3 RAP
generated: 12 Aug 2010
UT
17:40:00
17:50:00
18:00:00
18:10:00
18:20:00
18:30:00
18:40:00

Chapter 5

Statistics

Now that we have found 50 events, we assume to be caused by an x-line reconnection process, they are statistically investigated in order to get more insight in both, our selected encounters and the physics of reconnection.
Our main demand has always been the correlated reversals of B_z and $|\mathbf{V}_{\perp x}|$. According to these two parameters we implemented two strategies to characterize an event:

B_z-criterion: during the event interval the times of minimum and maximum magnetic field z-component are identified. The value of minimum and maximum flow are taken at exactly these times. They are not calculated separately, thus do not necessarily correspond to the absolute minimum and maximum during the period.

V_x-criterion: instead of the magnetic field component the times of minimum and maximum flow velocity are checked and the value of B_z is taken at these times.

So there are two different ways of treating each event. For each strategy a datasheet or matrix of the 50 final events was generated that lists all important parameters taken at the time according to the chosen criterion. It also shows the datagaps as NaN-entries, which cannot be used in statistics.
Statistics are performed for spacecraft 1 and 4 only. Cluster 2 provides no plasma data and Cluster 3 is too noisy in its plasma parameters.
Also not every plot of the statistic makes use of data from all 50 events because there are several data gaps, which diminish the available set of values.

Δt-Plot

An interesting question is, whether earth or tailward flow is detected first. For this purpose the time difference of the flows was calculated.

$$\Delta t = t_{\text{earthward}} - t_{\text{tailward}} \tag{5.1}$$

Negative values are received for events beginning with earthward flow. For both spacecraft and in both criteria the histogram-plots show an asymmetry. In each

plot there are more events detected beginning with tailward high speed flow. The result can also be used as an estimate of the average time of a reconnection event.
Cluster 1 detects in B_z-criterion 10 events beginning with earthward flow and 36 events start with tailward flow in. For the V_x-criterion the ratio is 6:40, for earthward beginning to tailward beginning flows.
For Cluster 4 the results are almost the same. 10 events are starting with earthward flow and 37 start with tailward flow in B_z-criterion and 5:42 in V_x-criterion.
The asymmetry is very clear in both criteria and for both spacecraft in the same sense.
The majority of detected events starts with tailward flow.

ΔV-Plot

Another histogram plot was created for ΔV, the difference in the absolute value of the tail and earthward flow-velocity in x-component.

$$\Delta \mathrm{V} = |\mathrm{V}_E| - |\mathrm{V}_T| \tag{5.2}$$

$|\mathrm{V}_E|$ is the earthward flow in x-direction and $|\mathrm{V}_T|$ stands for tailward flow.
An interesting fact is that the results depend on the criterion used to determine the flow velocity. For the V_x-criterion there are almost twice as much events with a positive value, thus a higher absolute earthward velocity. For spacecraft 4 this is even clearer than for Cluster 1.
The result is completely different in B_z-criterion. There is obviously no asymmetry. For spacecraft 4 there are even more events with higher tailward velocity, see table 5.1
This also proves that the criteria cannot be treated equally. The result of the Vx-criterion is that the earthward flow velocity is higher than tailward flow speed.
In the table (5.1) the ratio of negative to positive ΔV-values is shown,
$\Delta V < 0 : \Delta V > 0$.

ΔV	SC1	SC4
B_z-criterion	19:21	24:23
V_x-criterion	15:26	16:31

Table 5.1: Ratio of negative to positive values ΔV for Cluster 1 (SC1) and Cluster 4 (SC4) in both criteria.

ΔE-Plot

The symmetry of the reconnection rate or the acceleration of the plasma jet was examined in a ΔE-histogram plot. Due to the fact that

$$\mathbf{E} = \mathbf{V} \times \mathbf{B} \tag{5.3}$$

$$\mathrm{E}_y = -\mathrm{V}_x \, \mathrm{B}_z \tag{5.4}$$

we only need to look at the y-component of the electric field. Is there a difference in the electric fields accelerating plasma in the outflow regions? Again this

is totally dependent on the criterion we use. In V_x-criterion the difference is significant. The electric field and so the acceleration earthward is stronger than in tailward direction. In B_z-criterion this is not the case.
To create a histogram-plot we proceeded as before.

$$\Delta \mathrm{E}_y = |\mathrm{E}_y|_E - |\mathrm{E}_y|_T \tag{5.5}$$

Again subscript E stands for earthward and T for tailward.
For Cluster 1 we at least have the same tendency in both criteria. In B_z-criteria there are 18 negative values and 22 positive, hence more events with stronger earthward acceleration. This is even clearer in V_x-criterion with a ratio of 11:30, negative to positive.
Cluster 4 shows ambiguous results. In B_z criteria the ratio is 26:21 and so a reversed tendency than before and than in V_x-criteria with a ratio of 21:26.
It seems that there is no asymmetry in the reconnection electric field between earthside and tailside.

$B_z \mathrm{V}_x$-Plot

Next we'll have a look at the events themselves. Do they really correspond to x-line encounters in both criteria? To show the correlation B_z was plotted over V_x. What is expected are data in second and fourth quadrant because here is for positive flow velocity $B_z > 0$ and respectively for negative flow velocity $B_z < 0$. All in all the data shows the desired characteristics.
There are several outliers. The outliers with higher absolute values in quadrant 1 and 3 are likely to be the signature of a plasmoid encounter or an o-line instead of an actual x-line. Outliers near the x-axis in B_z-criteria can be reduced if small absolute B_z-values are sorted out and only events with higher $|B_z|$ are retained. Concerning the outliers, it is found that in 3 of 4 plots the number of earthward travelling plasmoids is smaller than the number of tailward moving plasmoids. Also they are not equally distributed. Only in B_z-criterion of Cluster 1 this trend is not found.
In general plasmoids move slower than pure x-line plasma flow. This is because the plasmoid is formed in between 2 x-lines, which accelerate flow in opposite directions. A moving plasmoid has to overcome the counteracting force of one of the x-lines to perform an effective translation in one direction. In B_z criterion it is more likely to include plasmoid signatures than in V_x-criterion. That's why we take results from V_x-criterion more serious in general.

j_y-Plot

To display the information on the current density, j_y was plotted over V_x. High current density means that the current sheet is thin.
To show different dependencies two different kinds of the plot were made. A **red-green color plot** and a **multicolor plot**.
One plot was colored depending on the B_z-value of the data. Green color shows positive B_z and red points denote negative B_z values. In this red-green plot it is immediately obvious, which data don't have the desired behavior in B_z-V_x-correlation. Red points on the positive semiaxis of V_x and green dots on its negative semiaxis correspond to B_x-values with opposite sign than their V_x-values and should be neglected.

Another plot was created, colored depending on the year the events occurred. This was done because of the different scale size of the tetrahedron each year. If the measurements are depending on the year, the current density is influenced by the spacecraft separation, due to the local measurement method. In that case one expects a linear dependency on the spacecraft distances, ranging from 200 km to 4000 km. During the years the separations of the spacecraft are as shown in the table.

The inter-spacecraft distances during the years 2001 until 2004 are in the table (5.2). In 2005 the tetrahedron was not regular. So events of 2005 were not included.

Year	**Separation [km]**
2001	2000
2002	4000
2003	200
2004	1000

Table 5.2: Scale size of the tetrahedron from 2001 to 2004

A correlation would therefore have to show the following pattern.
2003 > 2004 > 2001 > 2002
blue > yellow > red > green

The values obtained from calculating mean and median values for each year are in the table (5.3).

SC1	2001	2002	2003	2004
Mean	6.3	4.2	8.5	4.3
Median	4.2	3.2	8.3	5.0
σ	5.4	3.2	7.8	1.9

SC4	2001	2002	2003	2004
Mean	6.6	6.5	8.8	7.7
Median	5.4	4.0	6.5	6.5
σ	4.8	13.2	9.3	4.1

Table 5.3: Results of the per-year calculation of j_y, including mean-values, median-values and standard deviation σ, for Cluster 1 (SC1) and Cluster 4 (SC4) measurements.

Both, mean and median values have indeed an appropriate pattern, but the dependency of j_y is not linear with distance. No typical scaling factor has to be introduced.

Negative j_y-values are not expected, but obtained. Small values can be explained by fluctuations and the insufficiency of the curlometer method. Strong negative values of the current density are more difficult to explain and need to be looked at in detail.

In 2003 the minimum separation of the Cluster of 200 km was present. A slight tilt of the current sheet can easily lead to detection of negative currents at such small distances of the tetrahedron-formation.

ΔZ-Plot

To find an estimate of the current sheet thickness a new parameter ΔZ was introduced. It is the ratio of the lobe magnetic field B_{lobe} and j_y.

$$\Delta Z = \frac{B_{\text{lobe}}}{j_y} \tag{5.6}$$

An approximation for the current density is

$$\frac{\Delta B_x}{\Delta z} = j_y \ . \tag{5.7}$$

Δz is the entire current sheet thickness and corresponds to the calculated ΔZ-value. To determine it, *mean values* are generated.
Additional the *median* was calculated, which is helpful to reduce the influence of outliers.
Due to the units of B_{lobe} [nT] and j_y [nA/m^2], a multiplicative factor of 796 is needed to get the result in [km].

In close vicinity of the x-line, in the diffusion region, MHD is not valid. The currents sheet in that region is believed to be very thin (200 km or thinner). The region, we have gained our event values from, is a little more away from the actual x-line, where plasma has been accelerated to almost Alfvén velocity, thus in the outflow region. Here the current sheet is already much thicker but still quite thin, due to its vicinity to an x-line.
We hope to find values thinner than the plasma sheet thickness. Within $x_{GSM} = -15\ R_E$ from Earth the plasma sheet thickness doesn't vary much with geomagnetic activity and is about 6 R_E at the midnight meridian. It has a concave shape and increases in size at higher absolute values of y-component, the dusk and dawn side to about twice its size. During active intervals the plasma sheet increases in between $-15\ R_E < x_{GSM} < -19\ R_E$ to an about 9 R_E thick sheet. The activity doesn't influence its size within 15 R_E from Earth. [BP90]

In the table (5.4) the results of the calculation are listed. Because there is no physical interpretation possible for negative values, we only took positive ΔZ-values into account in the calculation. The mean value shows a thickness clearly above 1 R_E, 1.64 R_E for Cluster 1 (SC1) and 2.54 R_E for Cluster 4 (SC4) measurements.
The results are much better considering the median-calculation of 1.04 R_E for Cluster 1 and even 0.73 R_E for Cluster 4. Here the influence of outliers is obviously reduced.

The curlometer method to calculate the current density involves all 4 spacecraft, their separation and the magnetic field measurements. To find out if the scale size of the formation influences the outcome, the new parameter ΔZ was

		SC1		SC4	
		[km]	$[R_E]$	[km]	$[R_E]$
Mean	allposi	10 441	1.64	16 212	2.54
	Vxmax	6 841	1.07	22 204	3.48
	Vxmin	13 321	2.09	10 442	1.64
Median	allposi	6 651	1.04	4 647	0.73
	Vxmax	5 215	0.82	4 741	0.74
	Vxmin	6 784	1.06	4 506	0.71
σ	allposi	17 893	2.80	40 258	6.31
	Vxmax	5 480	0.86	56 131	8.8
	Vxmin	23 318	3.65	11 896	1.86

Table 5.4: Calculated values of mean and median ΔZ for Cluster 1 (SC1) and Cluster 4 (SC4) data. In the *allposi*-calculation all positive ΔZ-values were used. *Vxmax* means that only positive values of the positive V_x-semiaxis were taken into account, while in *Vxmin* only positive ΔZ-values of the negative V_x-semiaxis were used. Standard deviation is included as σ.

considered to show how much the spacecraft distances affect the result, by comparing results of different years to each other.
Again different colored plots were used.
The **red-green colored plot** was used to make the wrong data visible. The red points on the left-hand side and the green points on the right-hand side, just like before in the previous j_y-plot. This time the data points were removed in the **multicolor plot**, with different color for different years. The removed points were not used in the calculation of any ΔZ.
ΔZ is also an estimator of a characteristic scale size factor for different years. If there is a constant factor associated with each year and differing from year to year, the current densities calculated for different years are not comparable to each other and have to be multiplied by it. In that case, the true current sheet thickness has not been found, as the ideal performance would be.

During the years the separations of the spacecraft have been shown in the previous section in the table (5.2). According to the table the expected influence of the scale size has to be of the following order:

2003 (200 km)< 2004 (1 000 km)< 2001 (2 000 km)< 2002 (4 000 km)
blue < yellow < red < green

Such an order was not observed.
The effect of this result is that the current sheet thickness was measured.
The calculated values of the current sheet thickness are all larger than any of the tetrahedron sizes during the years. For this reason the spacecraft-separation has little influence on the measurement. Besides higher current sheet thickness also guarantees the applicability of the curlometer method, because $L > R_{ij}$, which means the phenomenon is larger than the separation.

Another feature, we wanted to inspect, is whether there is a difference in the current sheet thickness in earthward and in tailward direction. To examine that

it is necessary to compare *Vxmax*-results, which assign the earthward directed side of the current sheet and *Vxmin*, the tailward directed sheet, both included in table (5.4).
An asymmetry cannot be verified in this study because of controversial results from different spacecraft. For Cluster 1 the tailward current sheet seems to be thicker, according to the results of *Vxmin*, while Cluster 4 shows the opposite tendency.

Next pictures of all plots are listed to show the results in detail. Instead of including all generated plots, only the most illustrative ones are shown. Units used in the plots are

quantity	unit
Δt	hh:mm
ΔE	mV/m
ΔV	km/s
B_z	nT
j_y	nA/m^2
B_{lobe}	nT
ΔZ	$\frac{1}{796}$ km

Table 5.5: Units of plot-parameters

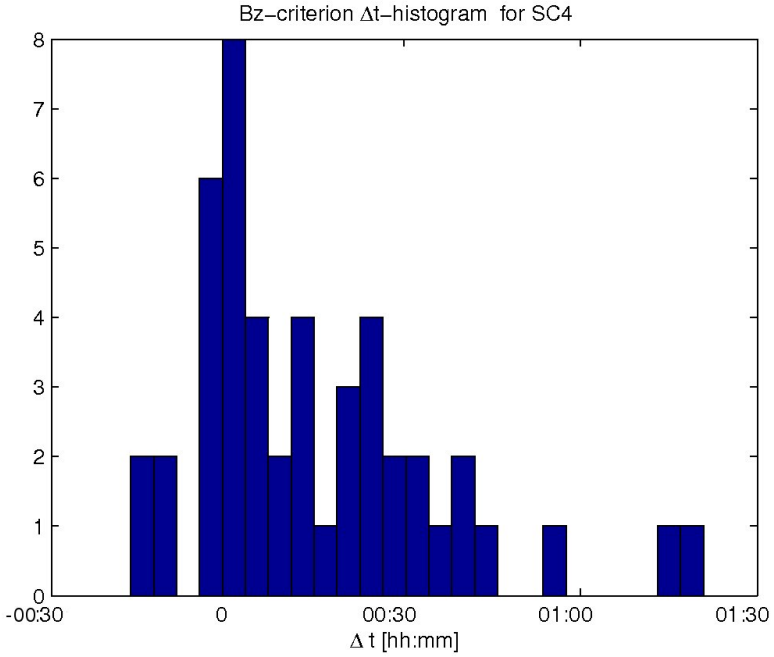

Figure 5.1: Δt-histogram of Cluster 4 in B_z-criterion

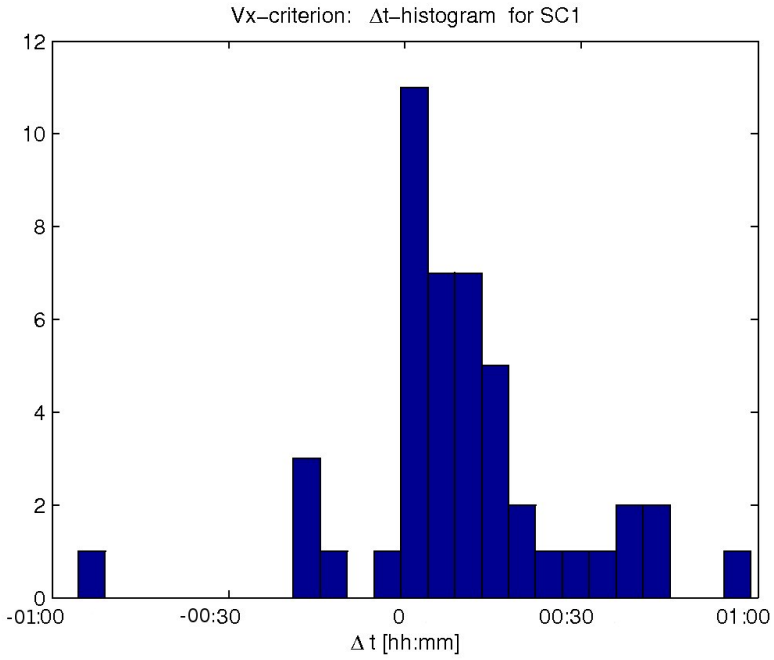

Figure 5.2: Δt-histogram of Cluster 1 in V_x-criterion

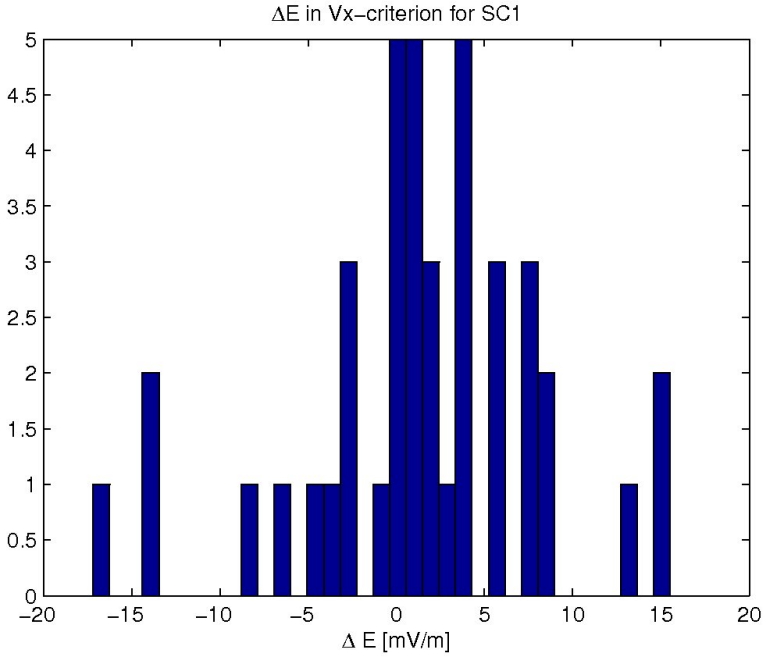

Figure 5.3: ΔE-histogram in V_x-criterion for Cluster 1

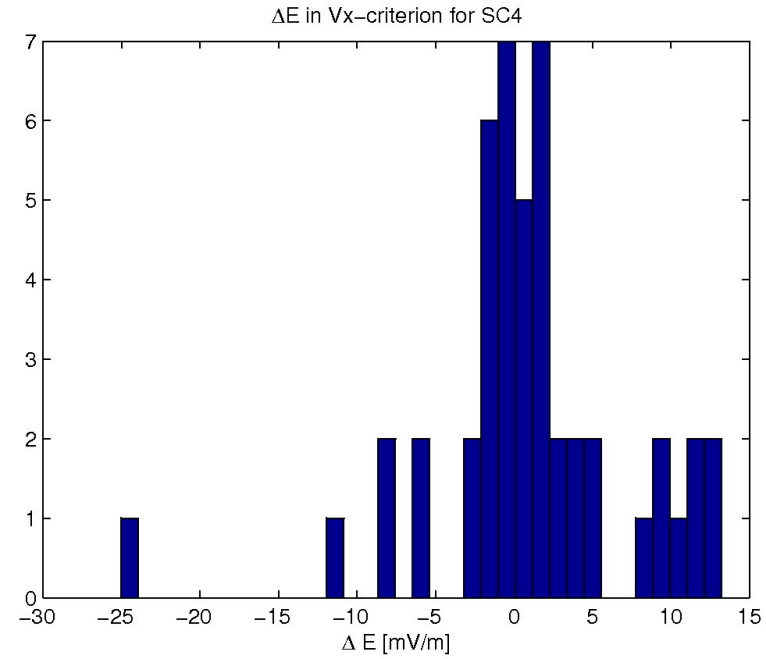

Figure 5.4: ΔE-histogram in V_x-criterion for Cluster 4

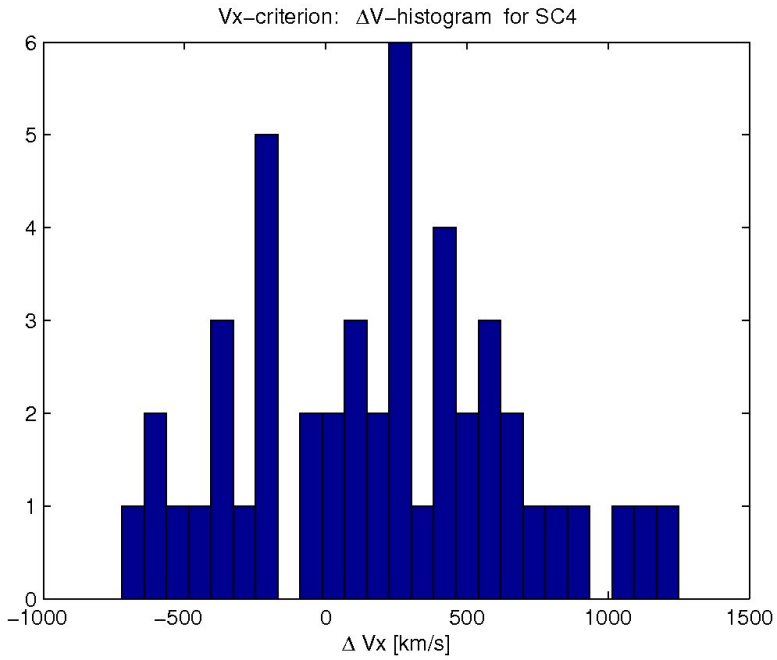

Figure 5.5: ΔV-histogram of Cluster 4 in V_x-criterion

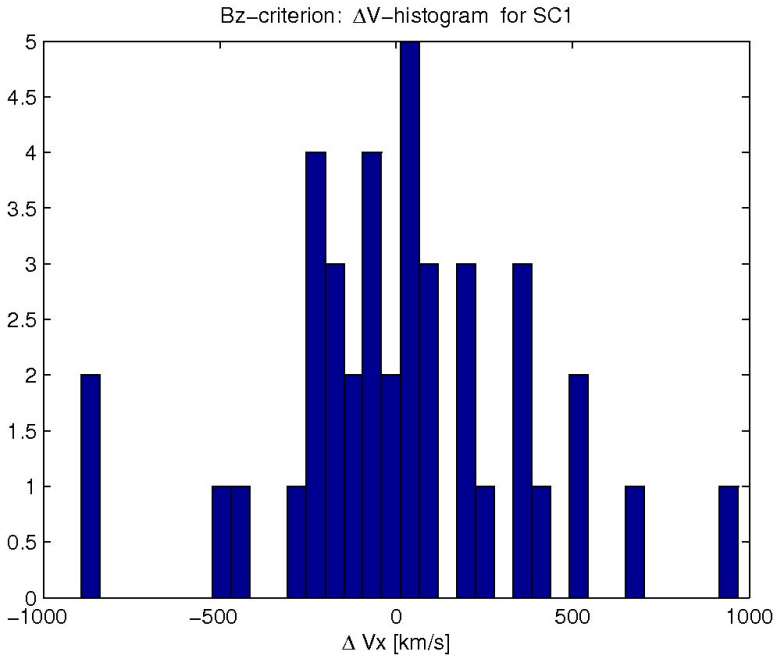

Figure 5.6: ΔV-histogram of Cluster 1 in B_z-criterion

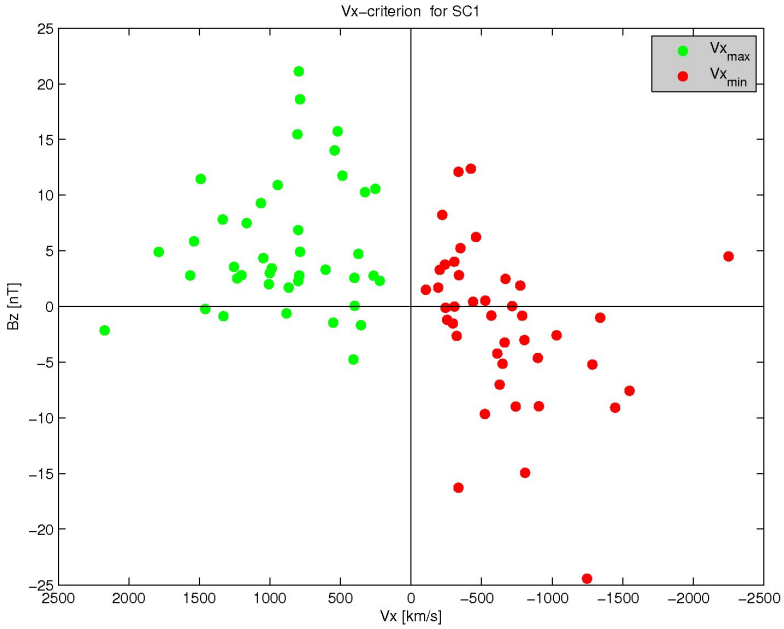

Figure 5.7: B_zV_x-plot of Cluster 1 in V_x-criterion

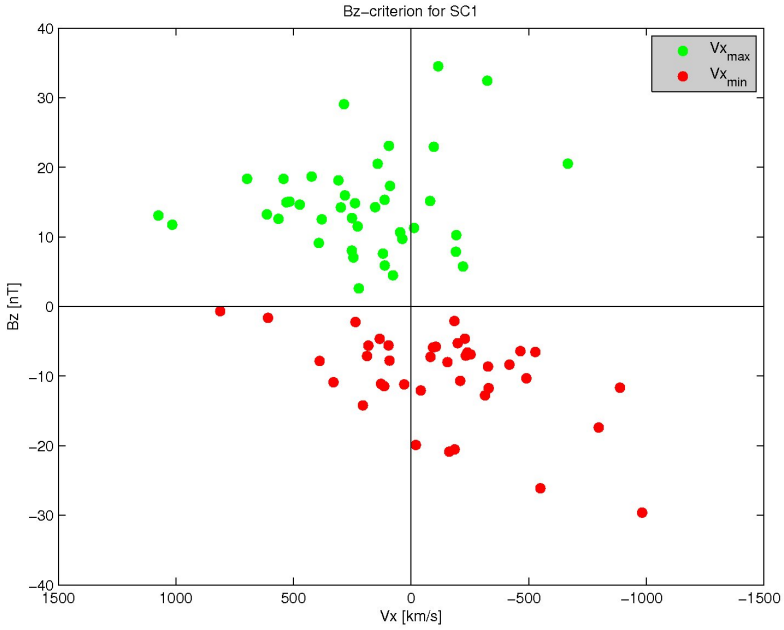

Figure 5.8: B_zV_x-plot of Cluster 1 in B_z-criterion

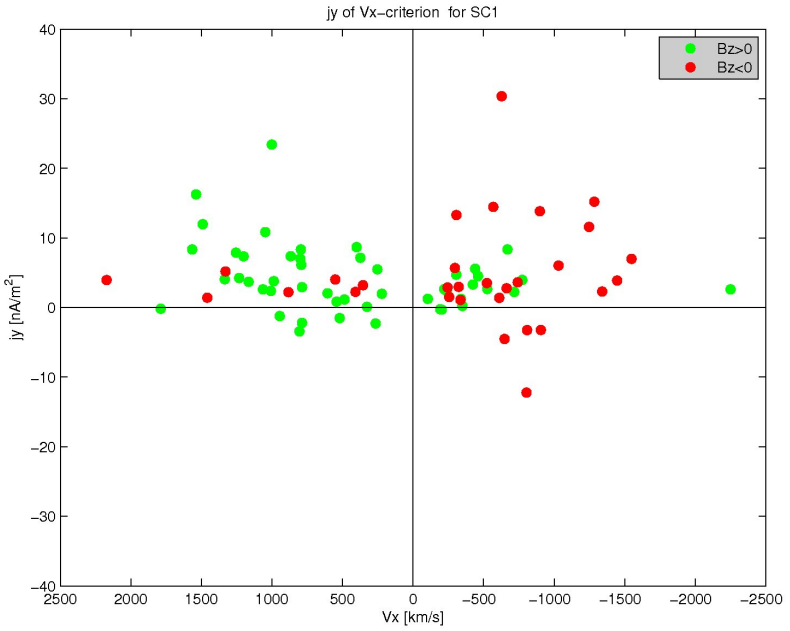

Figure 5.9: j_y in V_x-criterion for Cluster 1, colored depending on B_z

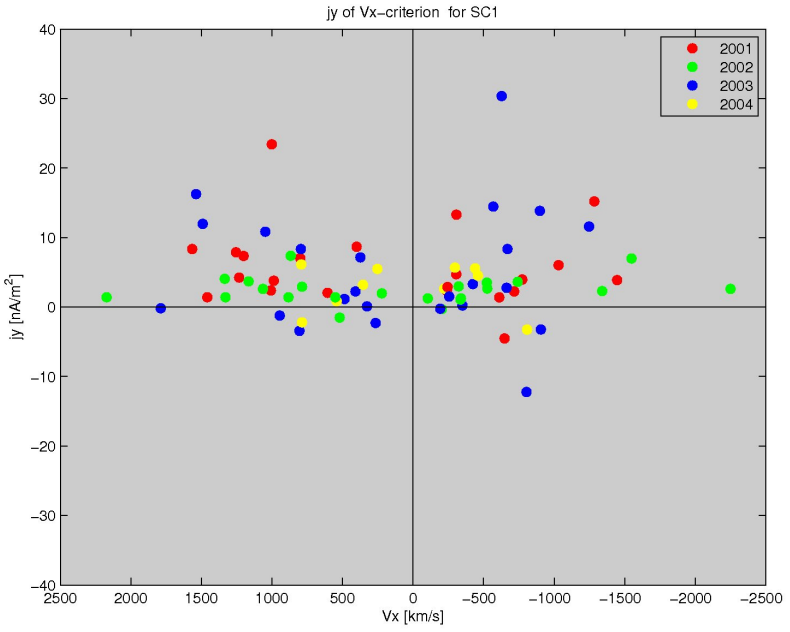

Figure 5.10: j_y in V_x-criterion for Cluster 1, colored depending on the year

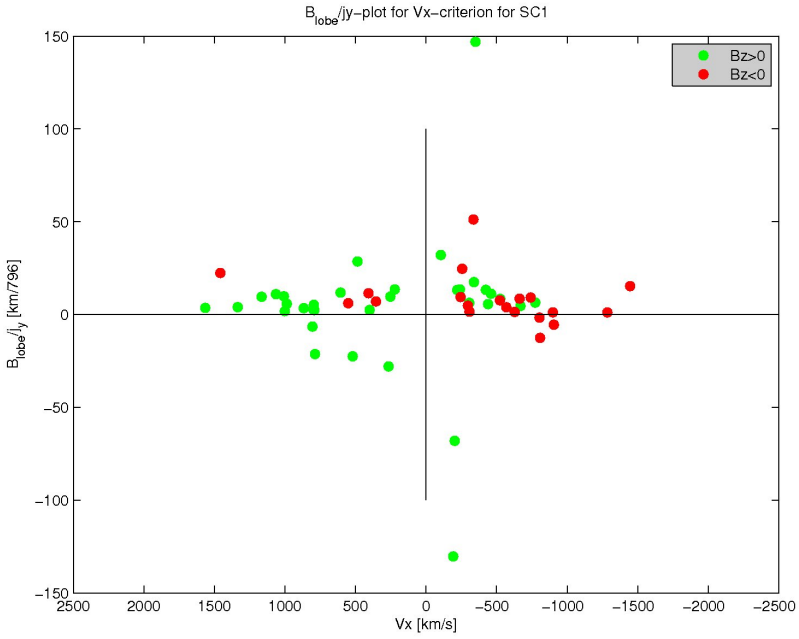

Figure 5.11: $\Delta X = B_{lobe}/j_y$ of Cluster 1 in V_x-criterion, colored depending on B_z

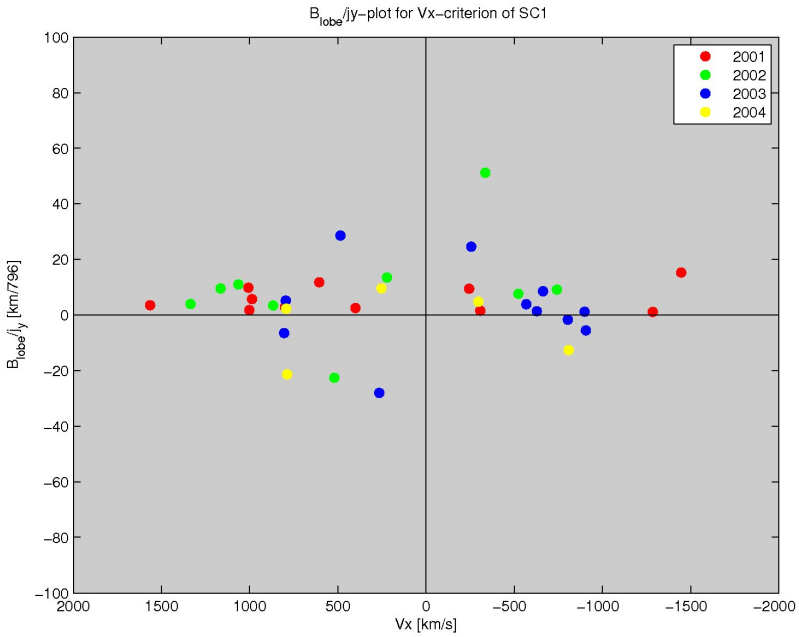

Figure 5.12: $\Delta X = B_{lobe}/j_y$ of Cluster 1 in V_x-criterion, colored depending on the year of measurement

Chapter 6

Summary

In this thesis a search of x-line events was performed, using Cluster Mission data of the years 2001 to 2007.
As search criteria a high plasma flow velocity $|V_{\perp x}| > 300\ km/s$ in x-direction together with simultaneously high plasma beta $\beta > 2$ were used.
The search algorithm was applied to Cluster 1, 3 and 4, because Cluster 2 provides no plasma data. Plasma data of the CIS-experiment has 4 second time-resolution, which corresponds to one spacecraft-spin.
Obtained data, meeting the criteria, was split into events, separated by at least 30 minutes from each other. These events were visually inspected and, after a sort out procedure, 50 probable x-line encounters were used to perform statistical investigations.
The automatic starting- and ending-time detection of each event was again visually checked and occasionally corrected.

To perform statistical analysis, two different methods were used, the B_z-criterion and the V_x-criterion. For each method maximum and minimum values occurring during the event of B_z and V_x, respectively, were taken. All further data of the event was taken at those times to perform the analysis. The criteria were compared to each other at the evaluation of each parameter.
In the statistical analysis the following results were obtained.

Events starting with tailward flow are present in higher number than events starting with earthward flow, as expected.

A comparison of earthward and tailward flow speed lead to inconsistent results, concerning the methods. While B_x-criterion did not show a difference, in V_x-criterion almost twice as much events with higher earthward flow velocity, than tailward flow speed, than events with higher tailward flow velocities occurred.

The histogram-plot comparing earthward to tailward electric field reveals that there is only a slightly higher field earthward of the x-line and so we concluded that the electric field doesn't show an asymmetry of tailward and earthward side.

To gain insight into the events themselves that were finally considered to be x-line encounters, B_z was plotted over V_x. An actual x-line event is expected to possess synchronous maxima and minima in B_z and V_x. To be an x-line event B_z and V_x at least must have the same sign at times of maxima or minima, as a consequence of the typical x-line structure $B_x V_x > 0$. In this plot events not meeting this criterion are easy to see. Not x-line like events with high absolute values are referring to o-line encounters, which have similar signature like x-line events, but opposite signs of B_z and V_x.
Also x-line events seem to be more complicated than originally expected and can consist of more than the pure x-line signature.
We conclude that in V_x-criterion the plasmoid or o-line encounters are less likely to occur than in B_z-criterion and thus we prefer results of the V_x-criterion.

To look at the currents in the neutral sheet during an event, j_y was plotted over V_x. Two kinds of the plot were made. One plot was colored depending on the sign of B_z, another depending on the year of measurement.
Current densities are relatively high with an average between 3.2 nA/m^2 and 8.8 nA/m^2, as expected of an x-line event.
Comparing mean and median values of different years, a pattern appropriate to the spacecraft-separation during the years was found, but the dependency is not linear.

An estimate of the current sheet thickness was found introducing a new parameter, ΔZ, being the ratio of lobe magnetic field B_{lobe} and current density j_y. ΔZ was plotted over V_x. A plot colored depending on the sign of B_z, as before, reveals the non x-line points, which are not taken into account in the following calculations. Also negative j_y-values were neglected.
Calculating mean and median, values in between 0.73 R_E and 2.54 R_E were obtained. Comparing measurements of the inflow- and outflow-region of the x-line, opposite tendencies for Cluster 1 and Cluster 4 are found.
In addition to that, a plot, colored depending on the year of measurement, was made. It shows that there is no pattern belonging to the year. One reason is that the thickness in the detection region is about 1 R_E, and therefore larger than the spacecraft-separation. For this reason, the curlometer method used is appropriate and the value obtained is indeed an estimate of the current sheet thickness.

Appendix A

Basic Derivations

A.1 One-fluid Theory

Plasma consists of electrons and ions. For simplicity the ion charge is assumed to be 1 with only one component of ions, the protons.

m_e, $q_e = -e$	mass and charge of electrons
m_i, $q_i = e$	mass and charge of protons

The continuity equation and the equation of motion is given separately for each component s, ions of electrons ($s = i, e$)

$$\frac{\partial n_s}{\partial t} + \nabla \cdot (n_s \ \mathbf{v}_s) = 0 \ , \tag{A.1}$$

$$\frac{\partial (n_s \mathbf{v}_s)}{\partial t} + \nabla \cdot (n_s \mathbf{v}_s \mathbf{v}_s) = -\frac{1}{m_s} \nabla \cdot \mathbf{P}_s + \frac{n_s q_s}{m_s} (\mathbf{E} + \mathbf{v}_s \times \mathbf{B}) \ . \tag{A.2}$$

Charges and Currents are defined by

$$\rho = e (n_i - n_e) \ , \tag{A.3}$$

$$\mathbf{j} = e (n_i \mathbf{v}_i - n_e \mathbf{v}_e) \ . \tag{A.4}$$

For a quasineutral plasma the total charge is zero, $\rho = 0$, thus $n_i = n_e = n$.

In magnetohydrodynamics plasma is treated as a conducting fluid. The fluid variables are a combination of its single components. Magentohydrodynamic equations derive from the upper two-fluid equations and the following definitions turning them into one-fluid equations

$$n = \frac{m_e n_e + m_i n_i}{m_e + m_i} , \tag{A.5}$$

$$m = m_e + m_i , \tag{A.6}$$

$$\mathbf{v} = \frac{m_i n_i \mathbf{v}_i + m_e n_e \mathbf{v}_e}{m_e n_e + m_i n_i} . \tag{A.7}$$

Continuity equation and equation of motion turn into the following equations in one-fluid theory

$$\frac{\partial n}{\partial t} + \nabla \cdot (n\mathbf{v}) = 0 , \tag{A.8}$$

$$\frac{\partial (nm\mathbf{v})}{\partial t} + \nabla \cdot (nm\mathbf{v}) = -\nabla \mathbf{P} + \rho \mathbf{E} + \mathbf{j} \times \mathbf{B} . \tag{A.9}$$

A.2 Magnetic Pressure

Taking the Lorentz force term $\mathbf{j} \times \mathbf{B}$ and using Ampère's law in MHD limit (IV) one gets

$$\mathbf{j} \times \mathbf{B} = -\frac{1}{\mu_0} \mathbf{B} \times (\nabla \times \mathbf{B}) , \tag{A.10}$$

$$\mathbf{j} \times \mathbf{B} = -\nabla \left(\frac{B^2}{2\ \mu_0} \right) + \frac{1}{\mu_0} \nabla \cdot (\mathbf{BB}) . \tag{A.11}$$

The first term on the right-hand side corresponds to the *magnetic pressure*

$$p_{mag} = \frac{B^2}{2\ \mu_0} . \tag{A.12}$$

The second term is the divergence of the *magnetic stress tensor* $\dfrac{\mathbf{BB}}{\mu_0}$. It causes tension and torsion in a conducting fluid. Taken from [BT96].

A.3 Particle Description

Microscopic particle characteristics are needed to decide, whether magnetohydrodynamic equations are valid or not. Here are the basic quantities.

Debye length λ_D:

$$\lambda_D = \sqrt{\frac{\epsilon_0 k_B T_e}{n_e e^2}} \tag{A.13}$$

Inside a sphere of radius λ_D the charge of the particles contained cancels. The Coulomb potential field of every charge is shielded by the other

charges. ϵ_0 is the free space permitivity, k_B is the Boltzmann constant. Electron and ion temperature are assumed to be about the same, $T_e \simeq T_i$, just like the single charged ion density and the electron density, $n_e \simeq n_i$.

Plasma frequency ω_{pe}:

$$\omega_{pe} = \sqrt{\frac{n_e e^2}{m_e \epsilon_0}} \tag{A.14}$$

Typical oscillation frequency of electrons about much heavier ions, caused by some external perturbation. The oscillation is motivated by the attempt to restore charge neutrality.

Cyclotronfrequency and Gyroradius: In a uniform magnetic field a charged particle with velocity V gyrates in a heliocoidal orbit around the magnetic field with a frequency depending on the field strength, the mass and charge of the particle. The *gyrofrequency* or *cyclotron frequency* is

$$\omega_C = \frac{qB}{m} \ . \tag{A.15}$$

For positively charged ions the frequency is positive, while electrons have a negative frequency, which is simply a gyration in the reversed direction. m is the particle mass.
the radius belonging to the motion is the *gyroradius* is defined as

$$r_g = \frac{mv_\perp}{|q|B} \ . \tag{A.16}$$

$v_\perp$ is the velocity perpendicular to the magnetic field.

List of Figures

List of Tables

Bibliography

[BP90] Baumjohann, W. ; Paschmann, G.: Geometry of the near-earth plasma sheet. In: *Journal of Geophysical Research* 95 (1990), Nr. A7, S. 10707

[BP07] Birn, Joachim ; Priest, Eric: *Reconnection of Magnetic Fields; Magnetohydrodynamics and Collisionless Theory and Observations*. Cambridge University Press, 2007. – ISBN ISBN 0–521–85420–2

[BT96] Baumjohann, Wolfgang ; Treumann, Rudolf A.: *Basic Space Plasma Physics*. Imperial College Press, 1996. – ISBN 1–86094–017X

[CAA] `http://caa.estec.esa.int/caa/home.xml`

[DDi] `http://www.daviddarling.info/encyclopedia/I/ionosphere.html`

[DDp] `http://www.daviddarling.info/encyclopedia/P/plasmasphere.html`

[DDV] `http://www.daviddarling.info/encyclopedia/V/Van_Allen_belt.html`

[ERS97] Escoubet, C. P. (Hrsg.) ; Russell, C. T. (Hrsg.) ; Schmidt, R. (Hrsg.): *The Cluster and Phoenix Missions*. Kluwer Academic Publishers, 1997. – ISBN 0–7923–4411–1

[esa] `http://sci.esa.int/science-e/www/object/index.cfm?fobjectid=23160`

[JM90] J.Chorin, A. ; Marsden, J. E. ; John, F. (Hrsg.) ; Marsden, J. E. (Hrsg.) ; Sirovich, L. (Hrsg.) ; Golubitsky, M. (Hrsg.) ; Jäger, W. (Hrsg.): *Texts in Applied Mathematics 4*. Bd. 4: *A Mathematical Introduction to Fluid Mechanics*. second. Springer Verlag, 1990. – ISBN 0–387–97300–1

[Ker71] Kertz, Walter: *Einführung in die Geophysik II*. Bd. 2. Hochschultaschenbuecher, 1971

[Khu96] Khurana, K.K.; Kepko E.L.; Kivelson M.G.; Elphic R.: Accurate determination of magnetic field gradients from four-point vector measurements. II. Use of natural constraints on vector data obtained

from four spinning spacecraft. In: *IEEE Transactions on Magnetics* 32 (1996), Sep 1, Nr. 5, S. 5193–9464. http://dx.doi.org/10.1109/20.538622. – DOI 10.1109/20.538622. – ISSN 0018–9464

[NAS] NASA

[PD00] Paschmann, Goetz (Hrsg.) ; Daly, Patrick W. (Hrsg.): *Analysis Methods for Multi-Spacecraft Data*. International Space Science Institute, 2000

[PEE+06] Perry, C. ; Eriksson, T. ; Escoubet, P. ; Esson, S. ; Laakso, H. ; McCaffrey, S. ; Sanderson, T. ; Bowen, H. ; Allen, A. ; Harvey, C.: The ESA Cluster Active Archive. In: *Cluster and Double Star Symposium* Bd. 598, 2006 (ESA Special Publication)

[rec] http://commons.wikimedia.org/wiki/File:Reconnection.gif

[RK95] Russell, Christopher T. (Hrsg.) ; Kivelson, Margaret G. (Hrsg.): *Introduction to Space Physics*. 1996. Cambridge University Press, 1995. – ISBN 0–521–45714–9

[SNR+08] Sharma, AS ; Nakamura, R. ; Runov, A. ; Grigorenko, EE ; Hasegawa, H. ; Hoshino, M. ; Louarn, P. ; Owen, CJ ; Petrukovich, A. ; Sauvaud, JA u. a.: Transient and localized processes in the magnetotail: a review. In: *Ann. Geophys* 26 (2008), S. 955–1006

[ST98] Suess, Steven T. (Hrsg.) ; Tsurutani, Bruce T. (Hrsg.): *From the Sun; Auroras, Magnetic Storms, Solar Flares, Cosmic Rays*. American Geophysical Union, 1998. – ISBN 0–87590–292–8

[Wik] http://en.wikipedia.org/wiki/Van_Allen_radiation_belt

Danksagung

Diese Arbeit entstand unter Leitung von Herrn Ao.Univ.-Prof. Dipl.-Ing. Dr.phil Martin Heyn am Institut für theoretische Physik, in Zusammenarbeit mit dem Institut für Weltraumforschung bei Doz. Dr. Rumi Nakamura, denen mein besonderer Dank gilt.

An dieser Stelle möchte ich mich sehr, sehr herzlich für die große Hilfe bedanken, die ich im Zuge dieser Arbeit erhalten habe. Ohne jene, die mich nicht nur motiviert haben, meinen Zeitplan einzuhalten und letztendlich diese Arbeit zustande zu bringen, wäre ich heute nicht in der glücklichen Lage, mein Studium zeitgerecht abschließen zu können.

Herr Professor Heyn sowie Frau Doz. Rumi Nakamura haben mich unglaublich unterstützt und mir die Überzeugung vermittelt, die ich selbst nie gehabt hätte, besonders um einen knappen Zeitplan einzuhalten. Außerdem haben sie mir in dieser Zeit eine Menge beigebracht und mich niemals mit einem Problem alleine gelassen.

Herr Professor Heyn hat mich besonders in theoretischen Fragen, wie auch in seinen Vorlesungen immer klar wird, auf die wichtigsten Punkte aufmerksam gemacht und mir Schlüsselfragen erklärt, sodass ich es wirklich leicht hatte. Außerdem gab er mir als Fachmann auf dem Gebiet der Reconnection gleich die richtigen Bücher in die Hand, aus denen ich die Zusammenhänge verstehen lernte. Seinem Zeitkonzept bin ich vielleicht manchmal hinterher gehinkt, aber ohne die Abläufe, die er mir vorgab, wäre es nie so produktiv voran gegangen. Außerdem hat er mir gezeigt, wie man eine solche Arbeit angeht und mir trotzdem viel Freiraum für meine eigenen Vorstellungen gelassen.

Doz. Dr. Rumi Nakamura bin ich bei einem ihrer Vorträge über die Cluster Mission 2006 zum ersten mal begegnet. Damals hat mich das Thema schon interessiert, aber ich hätte nicht gedacht, dass ich selbst einmal die Möglichkeit bekomme mitzuarbeiten. Als ich Sie dann vor einem Jahr bei einem anderen Vortrag auf mögliche Diplomarbeiten ansprach, war sie unglaublich entgegenkommend und hat mich sofort kontaktiert, ohne mich vorher einem langen Auswahlverfahren zu unterziehen. Obwohl es mir nicht möglich war den ursprünglich geplanten Themenschwerpunkt zu bearbeiten, war die Zusammenarbeit immer extrem produktiv, auch wenn ich es vielleicht nicht immer geschafft habe die Aufgaben perfekt umzusetzen. Auch zeitlich hat Sie mir immer geholfen, damit ich die Ziele nicht aus den Augen verliere, und eine Menge von ihrer eigenen Zeit dafür geopfert. Ich glaube doch viel davon profitiert zu haben und es war

ein sehr interessanter Einblick in ein ihr Spezialgebiet und das wissenschaftliche Arbeiten. Als Forscherin, aber auch als Mensch, wird sie mir immer ein Vorbild sein.

Dr. Martin Volwerk, der mir während dieser Zeit das Zimmer geteilt hat, ist ebenso ein wichtiger Ansprechpartner gewesen und ohne ihn wäre die Arbeit wahrscheinlich nur halb so gut geworden, weil er mir immer geholfen hat, wenn ich nicht weiter wusste, egal um was es ging. Mit seiner wissenschaftlichen Erfahrung, hat er mir klar gemacht, dass manche Dinge ganz einfach sein können, die ich selbst nie so erledigen hätte können, besonders auch wenn es um MATLAB ging. Auch er war immer für mich da und hat mir viel Zeit geopfert. Nicht zu vergessen, dass er auch ein sehr netter Arbeitskollege ist und es mit ihm im Zimmer immer lustig war.

Meiner Familie möchte ich danken, dass sie mich tatkräftig unterstützt und ebenfalls motiviert hat nicht aufzugeben und dass sie immer für mich da ist. Besonders auch, dass ich nie belastet war mit Kleinigkeiten, obwohl ich oft wichtiges in dieser Zeit vernachlässigt habe.

Nicht zu vergessen meine Freunde und Studienkollegen, die mir während des Studiums und besonders während meiner Diplomarbeit beiseite gestanden sind und ein Netzwerk bildeten, dass das Arbeiten erleichtert hat. Auch von ihrer Seite habe ich viel Motivation und Information bekommen, um weitermachen zu können.

Dem gesamten Team, sowohl am IWF als auch an der TU-Graz, das für die Abwicklung der Vorgänge zuständig ist, die nötig sind um eine Diplomarbeit durchzuführen und ein Studium abschließen zu können, möchte ich danken, für ihr Verständnis und schnelles Handeln, weil es bei mir doch knapp war Fristen einzuhalten, und mir niemals Steine in den Weg gelegt wurden.

Relindis Rott
November 15, 2010